



Australian Government
Bureau of Meteorology

The Centre for Australian Weather and Climate Research
A partnership between CSIRO and the Bureau of Meteorology



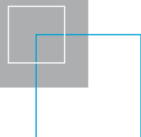
CAWCR Research Letters

Issue 2, July 2009

P. A. Sandery, T. Leeuwenburg, G. Wang, A. J. Hollis (editors)



www.cawcr.gov.au



ISSN: 1836-5949

Series: Research Letters (The Centre for Australian Weather and Climate Research); Issue 2.

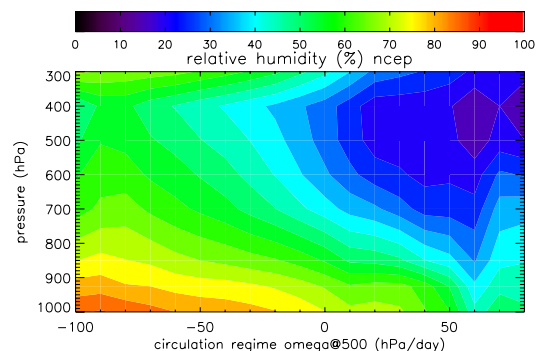
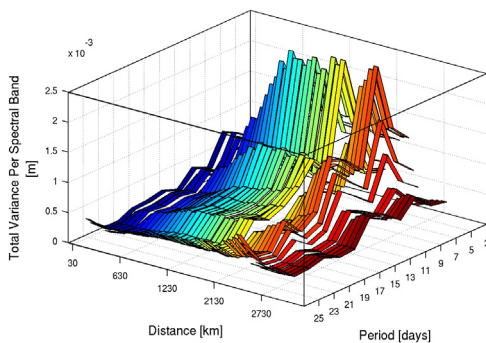
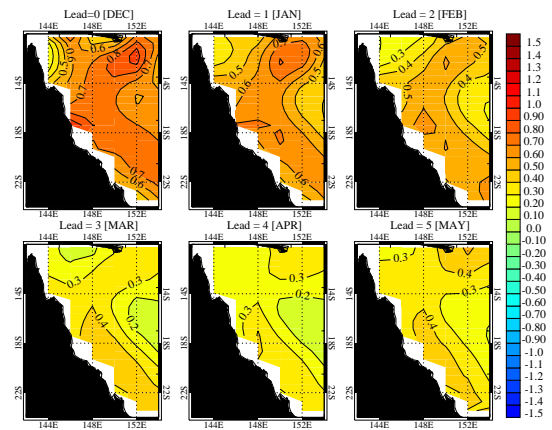
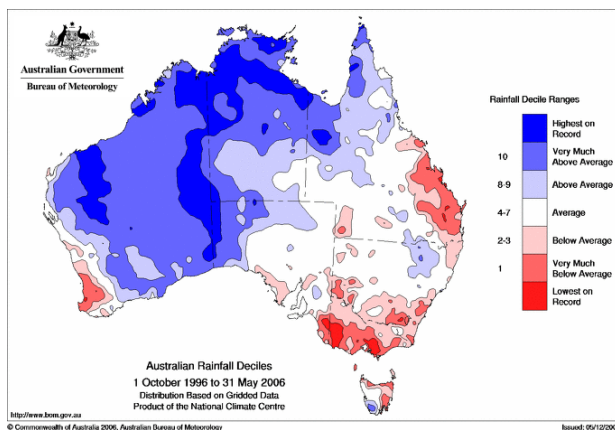
Copyright and Disclaimer

© 2008 CSIRO and the Bureau of Meteorology. To the extent permitted by law, all rights are reserved and no part of this publication covered by copyright may be reproduced or copied in any form or by any means except with the written permission of CSIRO and the Bureau of Meteorology.

CSIRO and the Bureau of Meteorology advise that the information contained in this publication comprises general statements based on scientific research. The reader is advised and needs to be aware that such information may be incomplete or unable to be used in any specific situation. No reliance or actions must therefore be made on that information without seeking prior expert professional, scientific and technical advice. To the extent permitted by law, CSIRO and the Bureau of Meteorology (including each of its employees and consultants) excludes all liability to any person for any consequences, including but not limited to all losses, damages, costs, expenses and any other compensation, arising directly or indirectly from using this publication (in part or in whole) and any information or material contained in it.

Contents

The continuing decline in South-East Australian rainfall: Update to May 2009	B. Timbal	4
Analysis of low latitude cloud properties in the ACCESS AMIP simulation – regime sorting using mid-tropospheric velocity	C. Franklin and M. Dix	12
Simulating the atmospheric transport of CO ₂ and SF ₆ using the UK Met Office Unified Model	R. M. Law and K. D. Corbin	18
Introducing the Natural Language Generation of Text Weather Forecasts in the GFE	T. Leeuwenburg	24
POAMA SST Predictions for the Great Barrier Reef: Summer 2008/2009	C. M. Spillman, O. Alves, D. A. Hudson and A. N. Charles	30
Weather-Band Coastal Sea Level Anomalies along Australia's Southern Shelves: Bluelink OceanMAPS	A. Taylor	35
Numbers and Genesis Locations of Tropical Cyclones in the NOAA IBTrACS Archive	I. G. Watterson	40



Editors: P. A. Sandery, T. Leeuwenburg, G. Wang, A. J. Hollis
Enquiries: Dr Paul Sandery p.sandery@bom.gov.au
 CAWCR Research Letters
 The Centre for Australian Weather and Climate Research
 Bureau of Meteorology
 GPO Box 1298K Melbourne VICTORIA 3001

CAWCR Research Letters is an internal serial online publication aimed at communication of research carried out by CAWCR staff and their colleagues. It follows on from its predecessor *BMRC Research Letters*. Articles in *CAWCR Research Letters* are peer reviewed and typically 4-8 pages in length. For more information visit the *CAWCR* website.

The continuing decline in South-East Australian rainfall: update to May 2009

Bertrand Timbal

Centre for Australian Weather and Climate Research

Bureau of Meteorology

b.timbal@bom.gov.au

Introduction

Most of South-Eastern Australia (SEA) has seen reduced rainfall since the late 1990s (National Climate Centre – NCC-, 2008). Murphy and Timbal (2008) (hereafter, MT08) described the ongoing dry conditions across most of southern Australia to 2006 and its many impacts; of particular concern for water resource management agencies have been recent record low inflows or river run-offs into the Murray-Darling Basin (MDBA, 2009).

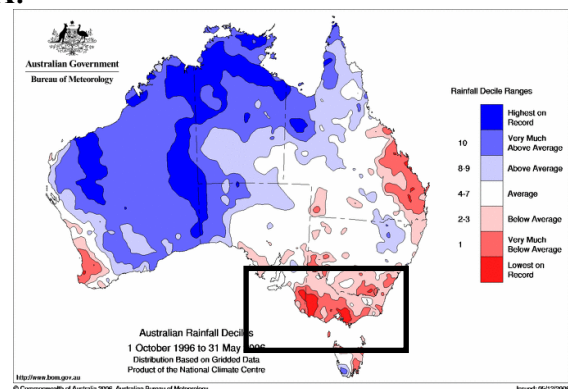
The South Eastern Australia Climate Initiative (SEACI) (Phase 1) was a 3 and a half year research program (2006-2009) dedicated in part to understanding and attributing the on-going rainfall decline (SEACI, 2007). The SEACI research program is about to embark on a new 3 year phase (SEACI-2) with a stated aim: “to enhance the understanding and improve predictions of the climate of south eastern Australia in order to better manage the impacts of climate change and variability across the region, with a focus on the impacts on water availability”. This note intends to contribute to the overall program goal by updating the description of the rainfall decline in SEA, its continuation since 2006 and changes in characteristics (i.e. magnitude, spatial extension and seasonality).

Worsening and broadening of the rainfall decline

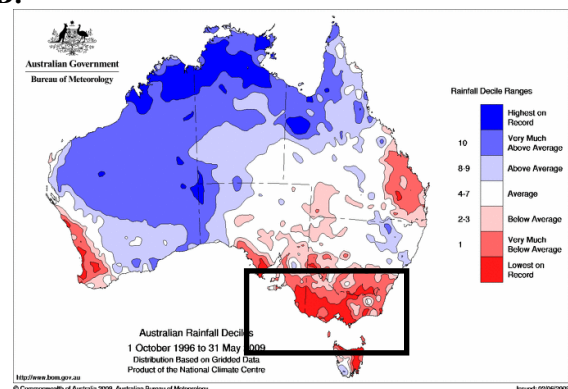
By May 2006, rainfall deciles across the Australian continent since October 1996 (Figure 1A) showed the clear emergence of a long-term rainfall deficit across SEA (within the area outlined by the black box: south of 33.5°S and

east of 135.5°E). In a by-and-large wet decade across the Australian continent, it was a significant negative anomaly, on par with a similar anomaly in size and magnitude in south-eastern Queensland. Smaller negative anomalies were also emerging in the south-west of Western Australia (SWWA) and north-eastern Tasmania. MT08 reported that SEA was experiencing one of its worst protracted droughts on record, although it was not the driest decade. A larger rainfall deficit was observed during World War II (WWII), from 1936 to 1945.

A:



B:



C:

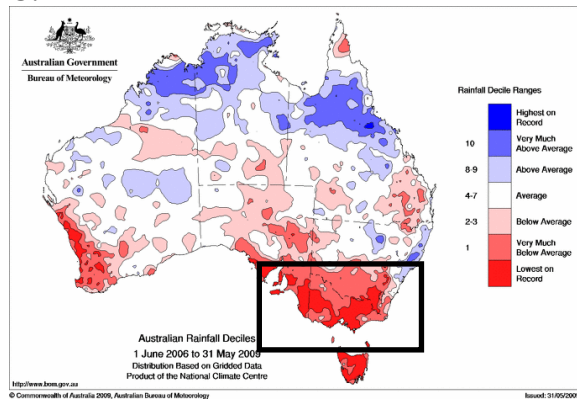


Figure 1. Total rainfall deciles across the Australian continent for October 1996 to May 2006 (A), updated to May 2009 (B) and for the additional 3 years from June 2006 to May 2009 (C). Deciles are expressed using the long-term climatology from 1900 to 2009. The box used for SEA average is shown in black (Maps courtesy of the National Climate Centre).

Figure 1B shows the same type of map except that it includes three more years and ends on 31 May 2009. The continent as a whole is still experiencing an above average rainfall period, but in general the areas suffering from long-term rainfall deficits have continued to be dryer than normal, displaying more severe anomalies. Arguably the situation in south-eastern Queensland is unchanged but the worsening is obvious across SEA and noticeable in the other southern dry regions (north and east of Tasmania and SWWA). The area under decile 1 now covers two thirds of the SEA box and the area affected by the largest rainfall anomalies on record has more than quadrupled. Seen in isolation, the latest 3 years (from June 2006 to May 2009, Figure 1C), not surprisingly, were very dry across most of southern Australia and in particular SEA: rainfall in the lowest decile was recorded across most of the SEA box with about half recording the lowest 3-years total rainfall on record.

Within SEA, the spatial expansion between 2006 (Figure 1A) and 2009 (Figure 1B) of the area affected by record low rainfall includes the south western part of eastern Australia (SWEA), as identified in earlier studies by Timbal and Jones (2008) and Hope et al. (2009) but now also includes regions further east along the northern

slope of the Great Dividing Range in eastern Victoria and southern New South Wales. The decile 1 rainfall area has extended from the south-west across two thirds of SEA, covering the entire Murray catchment (the Murray river and tributaries are shown on Figure 4) and leaving only the north eastern corner with average rainfall and small pockets further south. Two small pockets showing no rainfall decline are worth mentioning: the southern part of the Mt Kosciusko National Park (in the lee of the main range) and an area north-east of Adelaide in the lee of the Southern Flinders Ranges. These two small regions in the lee of significant orographic features (which tends to enhance rainfall on the western slopes and decrease rainfall on the eastern sides in westerly flows) reinforces the impression that the highest rainfall decline is linked to a weakening of the dominant westerly flow as expected from a rainfall deficit whose temporal signature is scattered across the wet autumn/winter/spring months.

Table 1. Mean and standard deviation (σ) of annual an autumn rainfall (in mm) over SEA for the on-going drought (Oct 96 to May 09) and the WWII drought (January 1935 to August 1947) and the long-term mean (1900 to 2008). Bold figures are statistically different at the 95% level.

	Oct 96 - May 09		Jan 35 - Aug 47		1900-2008	
	Mean	σ	Mean	σ	Mean	σ
Annual	503.6	82.7	511.7	102.5	566.5	107.4
Autum	99.7	31.0	120.5	32.5	132.4	49.6

As of May 2009, the twelve-and-a-half year rainfall average of $503.6 \text{ mm}\cdot\text{year}^{-1}$ (from October 1996) is now the lowest within the instrumental period; the previous lowest being $511.7 \text{ mm}\cdot\text{year}^{-1}$ before and during WWII (January 1935 to August 1947) (Table 1). It remains the case that the autumn rainfall decline is the most significant component of this decline: a 25% rainfall reduction from the long term mean (99.7 mm versus 132.4 mm) which accounts for just under 60% of the total rainfall decline and is significant at the 95% level. As noted in MT08, the strong autumn signature differs from the WWII protracted drought. Another difference is the very low inter-annual variability ($\sigma = 82.7 \text{ mm}$ compared to 107.4 mm for the long-term climatology versus 102.5 mm during WWII). It was then suggested (MT08) that the absence of

very wet years in the recent period, combined with the autumn signature and the on-going surface warming across SEA could have contributed to the significant consequences of the rainfall deficit in terms of river run-off across SEA compared to the WWII period.

Changes in seasonality of the rainfall decline

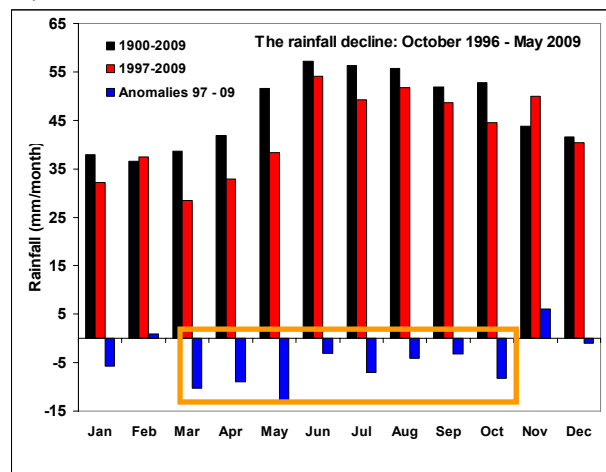
The autumn signature of the on-going protracted drought is still dominant with March, April and May recording the largest month by month anomalies in absolute values (Figure 2A). However, an evolution is noticeable compared to the similar analysis in 2006 (Figure 4 in MT08). There is now a continuum of 8 months from March to October showing a rainfall deficiency (outlined with an orange box). These 8 months include the entire wet season (May to October) where, over the 110 year long record period, 58% of the annual rainfall occurred. During the WWII period, there were also 8 continuous months with negative rainfall anomalies covering the wet season, but also extending into spring rather than earlier in autumn as in the current period (Figure 2B).

Whereas MT08 did find a rainfall increase in June, this is not the case in the analysis we give here for two reasons. Firstly, we have updated the recent period to May 2009 and June rainfall in 2006-2008 was 25% lower than the long term average. Secondly, we have changed the reference period from the World Meteorological Organization (WMO) recommended standard 1961-90 to the entire high quality instrumental period, 1900-2009. It contributed to the June abnormality since June was not noticeably wetter during the wet 1961-1990 period. In addition, since the WMO standard was a very wet 30-year period, it gave an inflated perspective of the rainfall decline. Using the long-term climatology (1900 to 2009) as a reference period, the decline is not as large but is now seen in all months from March to October.

In terms of the seasonality of the rainfall decline, since 1996, 11 out of 13 autumns have been drier than the long term average (including 2009), in contrast to 8 out of 12 winters and 6 out of 12 springs. Drier winters are equally distributed across the 12 years, although the last 3 winters

(2006, 2007 and 2008) have all been below average and have contributed to the very large recent anomalies. But a drying trend in spring is now emerging with spring rainfall below the long term average 6 times during the last seven years (2002-2008).

A:



B:

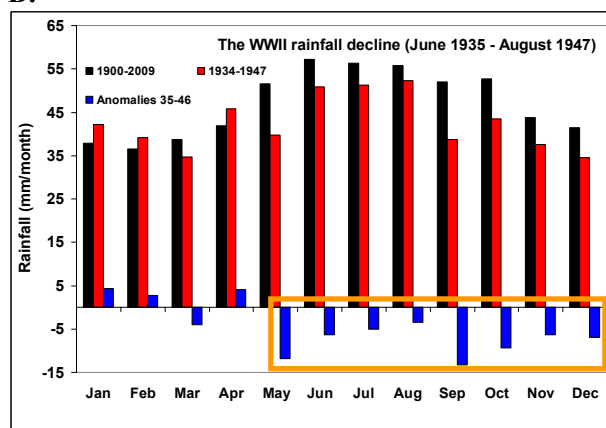


Figure 2. Monthly mean SEA rainfall for the long-term climatology (black bars), for the on-going protracted drought (red bars in graph A) and during the World War II protracted drought (red bars in graph B); changes from the long term climatology are shown as blue bars. The continuous months with negative rainfall anomalies are outlined with orange boxes.

Splitting the rainfall decline across the 3 seasons which surround the winter half year (excluding summer when rainfall anomalies are small and inconsistent), the growing contribution to the decline from spring is evident (left column in Figure 3).

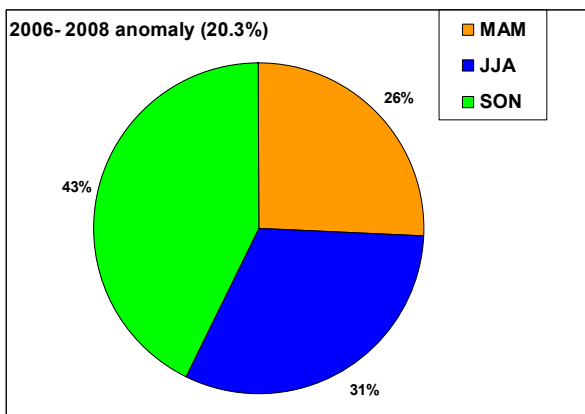
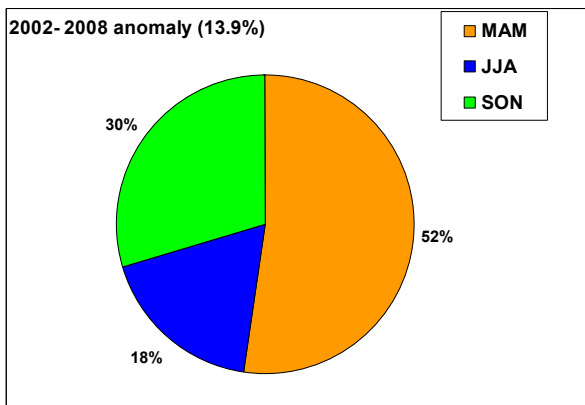
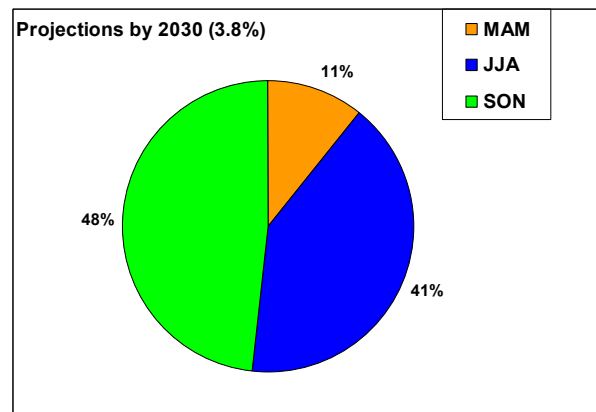
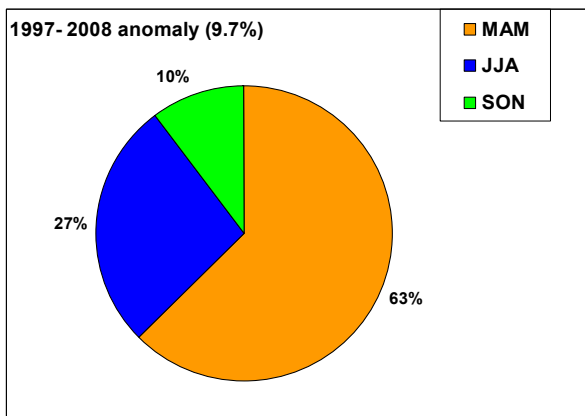
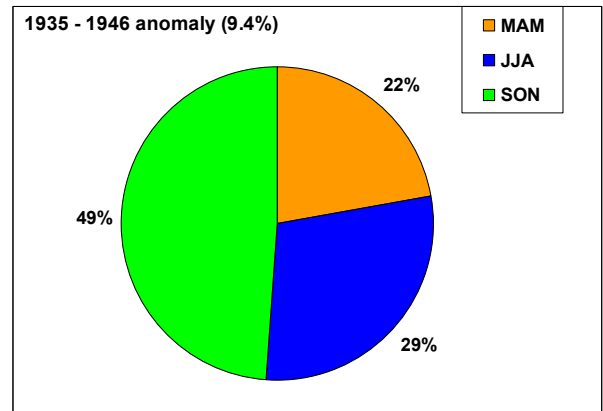
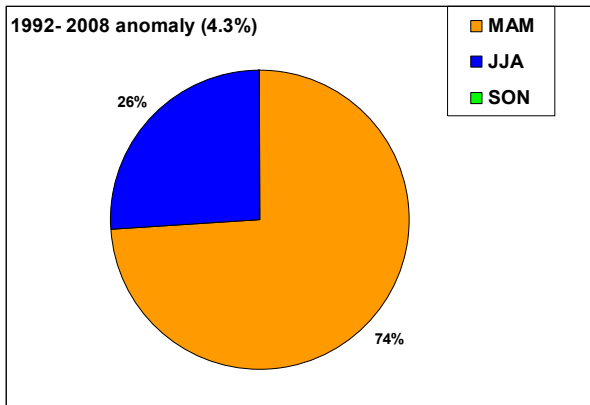


Figure 3. Seasonal split of the rainfall anomalies for the on-going protracted drought, considered since 1992 (top left), since 1997 (second left), since 2002 (third left), during the last 3 years (bottom left), the WWII protracted drought (top right) and climate change future projections (bottom right). In all graphs, summer anomalies, either negative or positive, are omitted and percentages are based on the 3 seasons displayed. The annual rainfall anomalies (shown in the top left of each graph) includes all four seasons and are calculated from the long-term 1900-2008 mean, apart from the future projections which are based on the 1980-2000 reference period.

A small but consistent rainfall decline can be traced as far back as 1992, when the autumn contribution (74%) dominates. For the period since 1997, the autumn contribution is still dominant (63%) but in the second half of that period it is somewhat less (52%) and only 26% over the last 3 years.

Note that this does not indicate a reduction of the autumn rainfall decline (it is -30.0 mm during the 1992-2008 period, -32.7 mm during the 1997-2008 period and -30.7 mm during the 2006-2008

period), but simply that its relative contribution to the overall decline is less. Indeed, the overall annual rainfall decline has grown from -4.3% over the 17 years (starting in 1992) to -9.7% since 1997 and was -20.3% during the last three years – mainly as a result of declines in other seasons particularly spring (it was -5.4 mm during the 1997-2008 period and -51.0 mm during the 2006-2008 period). The split of the anomalies between the three seasons during 2006, 2007 and 2008 is similar to what was observed during WWII. It is also similar to the expected changes due to greenhouse gas emissions in the near future based on the IPCC-AR4 model using all emission scenarios available by 2030 for grid boxes covering SEA (CSIRO and BoM, 2007). Although the seasonality of the rainfall anomalies in the latest period resembles future projections of rainfall in SEA, the magnitude of the recent decline (about 20%) far exceed even the worse climate model projections (the median of the projections or “best guess” is a 3.8% decline by 2030 compared to the 1980-2000 reference period).

As part of the SEACI program, the role of key modes of variability in the on-going drought was evaluated, particularly those in tropical oceans: the El Niño Southern Oscillation (ENSO) in the Pacific and the Indian Ocean Dipole (IOD). Although, these modes are known to be important drivers of the Australian (including in SEA) climate (McBride and Nicholls, 1983; Nicholls, 1989), it was noted that their impact is very weak in autumn where nearly two thirds of the rainfall decline has occurred (Timbal and Murphy, 2007). Therefore both the ENSO and IOD drivers are unlikely to have contributed significantly to the rainfall decline up to 2006. On the contrary the rise of Mean Sea Level Pressure (MSLP) across southern Australia (Timbal and Hope, 2008) and in particular the intensification of the Sub-Tropical Ridge (STR) as diagnosed by Drosowsky (2005) was found to be associated with a very sizeable part (about 70%) of the rainfall decline in SEA (Timbal et al., 2007). It is therefore noticeable that the area with the largest rainfall deficit (Figure 1) coincides closely with the area showing the biggest negative influence of the STR intensity on rainfall (Figure 4) thus strongly suggesting a role for the STR intensification on the on-going drought across SEA. Recent studies have noted global scale

changes in the extent of the tropics, and the extent and intensity of the Hadley circulation. The tropics appear to be getting wetter over time (Allan and Soden, 2007), they appear to be expanding (Seidel et al., 2007), and the Hadley circulation also appears to be expanding (Lu et al., 2007). This suggests that the STR may be part of a much larger scale change in the global scale circulation, particularly as it provides a physical link between the decline in rainfall in SWWA and that now seen in SEA (Hope et al., 2009).

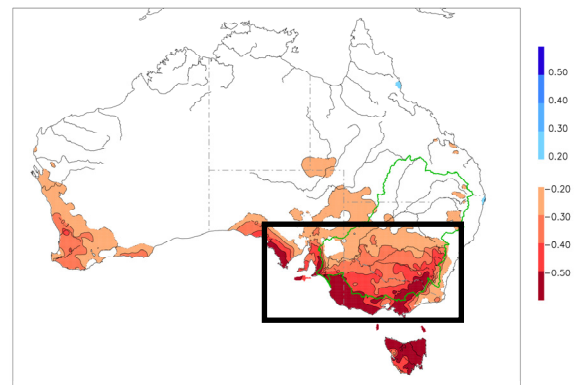


Figure 4. Detrended correlations between the Sub-Tropical Ridge intensity and rainfall across Australia for all months, correlations significant at the 95% level and above are colour shaded.

However, in light of the shift toward a larger spring rainfall anomaly in the last 3 years, a season where both ENSO and IOD are well formed with a sizeable influence on SEA rainfall (Timbal and Murphy, 2007), it is worth reviewing the recent phases of both modes of variability. Monthly normalised anomalies for ENSO indicators and the IOD Mode Index can be accessed from the BoM NCC web site:

<http://www.bom.gov.au/climate/ensoi/indices.shtml>.

In the case of the tropical Pacific Ocean, the period from June 2006 to May 2009 comprised both positive and negative phases of ENSO with a weak El Niño event in 2006/07 followed by moderate La Niña event in 2007/08. A further negative La Niña-like anomaly followed in 2008/09. Overall, there has been no bias toward either phase. In addition, the 3 years rainfall decile map (Figure 1C) is not consistent with the expected rainfall influence from either El Niño or La Niña events across Australia:

<http://www.bom.gov.au/climate/ensoi/ensorain.shtml>.

Therefore, it is unlikely that ENSO variability has

contributed to the worsening of the drying trend in SEA.

In the case of the tropical Indian Ocean, the period from June 2006 to May 2009 was notable for a bias toward positive phase of the IOD. Three positive IOD events were recorded in that period; this is remarkable and only happens once before in the instrumental record at the end (1944, 1945 and 1946) of the WWII dry decade (Meyer et al., 2007). In addition, the 3 years rainfall decile map has some similarities in particular across Eastern Australia including SEA, with the known impact of IOD on Australian climate which peaks in late winter early spring (Figure 5). This suggests that the Indian Ocean variability has likely contributed to the worsening of the rainfall decline during the last three years and in particular the additional shortfall in spring on top of the continuing autumn decline. This importance of the IOD on the observed SEA rainfall decline since 1997 should not be overestimated since it is limited to the latter part of the wet season (i.e. the spring contribution of the rainfall decline since 1997 is 10%, Figure 3). However it is worth noting and monitoring since climate model future projected rainfall decline in SEA has a strong spring signature (Figure 3).

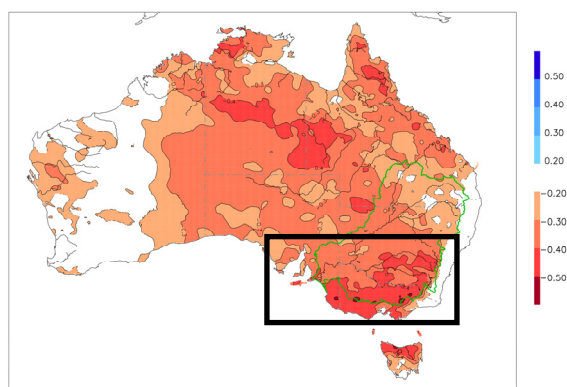


Figure 5. Detrended correlations between the Indian Ocean Dipole and rainfall across Australia for August to October, correlations significant at the 95% level and above are colour shaded.

Besides tropical influences, the role of the Southern Annual Mode (SAM), the largest mode of variability in the southern hemisphere, is also worth monitoring. The influence of a positive phase of SAM on SEA rainfall is highly seasonal: positive in summer, negative in winter with no influence in autumn (Timbal et al., 2007). The

lack of influence in autumn was pointed out as the main reason why SAM is unlikely to be an important contributor to the SEA rainfall decline (Timbal and Murphy, 2007), however that influence is worth monitoring since another study suggests that SAM is the main explanation for the southern Australia rainfall decline (Nicholls, 2009). Linear trends were calculated month by month (and for 3-month running means) from the Marshall (2003) index based on observed MSLP (<http://www.nerc-bas.ac.uk/icd/gjma/sam.html>) at selected stations and the Climate Prediction Centre (CPC) SAM index based on 700 hPa geopotential height (Figure 6).

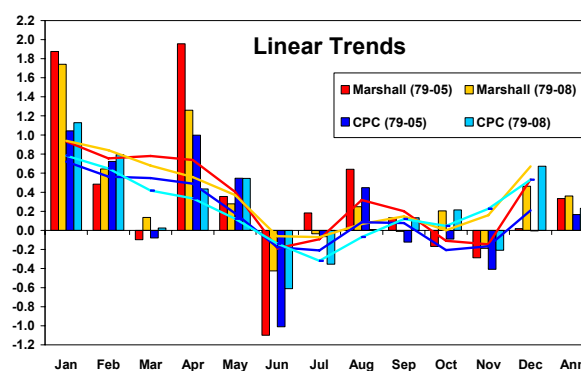


Figure 6. Linear trends month by month (bars) and for 3-month running means (lines) using Marshall (red colors) and CPC (blue colors) SAM indices from 1979 to 2005 (dark colors) and from 1979 to 2008 (light colors).

Linear trends are calculated since 1979 (the CPC calculation based on reanalyses are considered unreliable prior to the satellite era) to 2005 and have been updated to the end of 2008. The overall picture is unchanged, the largest trends are observed in summer and autumn (when upward trends should have a positive influence on SEA rainfall). In the season where SAM has a negative influence on SEA rainfall (June-July-August), there are no long-term trends in SAM. It is worth noting that individual months with the largest trends (either positive: April or negative: June) up to 2005 have seen these trends being reduced as more years are included. With time, some of the largest random anomalies inevitable with linear trends calculated month by month on short periods are being eroded. It is likely that the positive values of SAM indices in June in 2006, 2007 and 2008 which contributed to reduce the

overall June trends also contributed to the dry months of June observed during these 3 years and discussed earlier. It is also interesting to note the emerging positive trend of the SAM in December (in both indices), which are consistent with the above average observed rainfall in December in 2007 and 2008 (but not in 2006 in the middle of an El Niño) and the positive influence of the positive phase of SAM in summer.

Conclusions

The long-term rainfall deficiency since October 1996 across South Eastern Australia (south of 33.5°S and east of 135.5°E) documented by MT08 was described as being severe but not unprecedented in the instrumental record. With an additional 3 years of below average rainfall, that statement is no longer true. The recent 12 year, 8 month period is the driest in the 110 years long record, surpassing the previous driest period during WWII. The spatial extent of the deficiency covers most of the south-western part of eastern Australia and extends along significant orographic features eastward and northward. The seasonal signature of the rainfall decline has also evolved. It remains dominated by a strong and highly significant autumn rainfall decline, but has been supplemented by recent declines in spring, particularly after 2002. The spring decline is the dominant feature of the very dry 2006-2008 period.

This change in the relative contributions by the autumn and spring seasons now more closely resembles the picture provided by climate model simulations of future changes due to enhanced greenhouse gases. However, the growing magnitude of the rainfall decline is far more severe than any of the IPCC-AR4 model projections except for the lowest deciles from the model uncertainty range, forced with the highest emission scenarios occurring later in the 21st century (2050 to 2070) (CSIRO and Bureau of Meteorology, 2007).

The most important characteristics of the ongoing rainfall decline (spatial extension, intensification and change in seasonality) are well aligned with the recent evolution of the STR and its known influence on SEA rainfall. Other large-scale influences were briefly evaluated. It appears unlikely that the ENSO mode of variability has

contributed to the worsening of the rainfall decline in the last 3 years. On the contrary, it appears likely that the Indian Ocean mode of variability (with three positive IODs in a row) may be linked to the strong spring signal in 2006-2008. However, that does not change the fact that the IOD is unlikely to be responsible for the largest component of the rainfall decline (the autumn part) and based on the limited evidence provided here, it is unclear whether the IOD is a contributor, or simply a covarying response to other factors. Finally, the long-term evolution of the SAM remains unlikely to explain the long-term decline in SEA due to the seasonal nature of the influence of SAM on SEA rainfall but its role (both positive or negative) is visible while updating month by month anomalies

One of the goals of the new SEACI program involves “*investigating the causes and impacts of climate change and climate variability across south eastern Australia*” This is now more relevant than ever, particularly as we are dealing with the worst rainfall deficit in the region within more than a century long instrumental record.

Acknowledgements

This communication arises from the involvement of BT in the South-Eastern Australian Climate Initiative (SEACI). The support of the funding agencies is acknowledged. Drs. Ian Smith (CAWCR/CSIRO), John Bally (CAWCR/BoM), Bradley Murphy (BoM/NCC), Harry Hendon (CAWCR/BoM), Julie Arblaster (CAWCR/BoM and NCAR) and Pandora Hope (CAWCR/BoM) have made useful comments to improve earlier versions of this communication. Rae Moran (Vic DSE) suggested updating the monitoring of the SAM influence.

References

- Allan, R.P. and B.J. Soden, 2007: Large discrepancy between observed and simulated precipitation trends in the ascending and descending branches of the tropical circulation, *Geophys Res Lett*, **34**, L18705, doi: 10.1029/2007GL031460
- CSIRO and Bureau of Meteorology, 2007, Climate Change in Australia, Technical report, Department of Climate Change, 148pp: <http://www.climatechangeinaustralia.gov.au>,
- Drosowsky, W., 2005: The latitude of the subtropical ridge over eastern Australia: the L index revisited, *Int J Climatol*, **25**, 1291-1299

- Hope, P., B. Timbal and R. Fawcett, 2009: Associations between rainfall variability in their southwest and southeast of Australia and their evolution through time, *Int J Climatol.*, in press
- Lu, J., G.A. Vecchi and T. Reichler, 2007: Expansion of the Hadley cell under global warming, *Geophys Res Lett*, **34**, L06805.
- Marshall, G.J., 2003: Trends in the Southern Annular Mode from observations and reanalyses, *J Clim*, **14**, 4134-4143
- McBride, J.L. and N. Nicholls, 1983: Seasonal relationship between Australian rainfall and the Southern Oscillation, *Mon Wea Rev*, **111**: 1998-2004
- Meyer, G., P. McIntosh, L. Pigot and M. Pook, 2007: The years of El Niño, La Niña, and interactions with the tropical Indian ocean, *J. Clim*, **20**, 2872-2880
- Murphy, B. and B. Timbal, 2008: A review of recent climate variability and climate change in south-eastern Australia, *Int J Climatol*, **28(7)**, 859-879
- Murray-Darling Basin Authority (MDBA), 2009: Murray River system, drought update: http://www.mdba.gov.au/system/files/MDBA_Drought_Update_April_2009.pdf
- National Climate Centre (NCC), 2008: Long-term rainfall deficiencies continue in southern Australia while wet conditions dominate the north, *Special Climate Statement*, **16**, 9pp: <http://www.bom.gov.au/climate/current/statements/scs16.pdf>
- Nicholls N., 1989, Sea surface temperatures and Australian winter rainfall, *J of Clim*, **2**, 965-973
- Nicholls N., 2009, Local and remote causes of the southern Australian autumn-winter rainfall decline, 1958–2007, *Clim Dyn*, DOI 10.1007/s00382-009-0527-6
- SEACI, 2007: South Eastern Australian Climate Initiative (SEACI) overview: <http://www.mdbc.gov.au/subs/seaci/docs/factsheets/SEACIfactsheet-overview.pdf>
- Seidel, D.J. and R.J. Randel, 2007: Recent widening of the tropical belt: Evidence from tropopause observations. *J Geophys Res*, **112**, D20113
- Timbal, B. and B. Murphy, 2007: Observed climate change in South-East of Australia and its relation to large-scale modes of variability, *BMRC Res Let* **6**, 6-11 http://www.bom.gov.au/bmrc/pubs/researchletter/reslett_06.pdf
- Timbal, B. and P. Hope, 2008: Observed early winter Mean Sea Level Pressure changes above southern Australia: a comparison of existing datasets, *CAWCR Res Let*, **1**, 1-7 <http://www.cawcr.gov.au/publications/researchletters/CAWCRResLets1.pdf>
- Timbal, B. and D. Jones, 2008: Future projections of early winter rainfall in South East Australia using a statistical downscaling technique, *Clim Change*, **86**, 165-187
- Timbal, B., B. Murphy, K. Braganza, H. Hendon, M. Wheeler and C. Rakich, 2007: Compare documented climate changes with those attributable to specific causes, *South-Eastern Australian Climate Initiative (SEACI)*, final report, project 1.1.2, 19 pp: http://www.mdbc.gov.au/subs/seaci/docs/reports/M112_FR07.pdf

Analysis of low latitude cloud properties in the ACCESS AMIP simulation – regime sorting using mid-tropospheric velocity

Charmaine Franklin^A and Martin Dix^B

^{AB}Centre for Australian Weather and Climate Research

CSIRO Marine and Atmospheric Research

charmaine.franklin@csiro.au

Introduction

Clouds play a key role in the global energy and water cycle. Depending on the cloud properties they can either warm or cool the climate through their effects on solar and terrestrial radiation. Due to the complexity of cloud microphysics and the difficulties with observing these small scale processes, the representation of clouds in global climate models (GCMs) continues to present a challenge for the modelling community. The radiative feedback from clouds remains a significant source of variation in the response of climate models to increases in global CO₂ concentrations. To have greater confidence in climate projections, both a better understanding of clouds and their feedbacks and an also improved representation in models are essential.

In this study the radiative impact of low latitude clouds in the ACCESS/UM AMIP (Atmospheric Model Intercomparison Study) simulation is evaluated using an analysis methodology made popular by Bony et al. (2004). The cloud radiative forcing (CRF) of the tropics depends on the distribution of the types of cloud, which is tightly coupled to the overturning circulation. The ascending motions of the large-scale circulation are associated with convective cloud systems producing shallow to deep cumuliform clouds, while the subsidence regions favour the formation of boundary layer clouds such as shallow cumulus and stratocumulus. The analysis technique used in this study decomposes the tropics into dynamical regimes by using the velocity at 500 hPa as a proxy for the large-scale atmospheric circulation. This methodology has the advantage of removing the effect of errors in the location and intensity of the simulated atmospheric circulation, which are not crucial to the radiative feedback processes in the model.

Data and model descriptions

An AMIP-type run from 1979-2000 was completed with a HadGEM1a like version of the ACCESS/UM model, run at a resolution of 1.975 by 1.25 degrees with 38 vertical levels. The model used in this study is the UM version 6.3, which includes:

- vertical advection, described by the semi-Lagrangian scheme of Davies et al. (2005);
- atmospheric longwave and shortwave radiation modelled by the Edwards and Slingo (1996) scheme;
- large-scale precipitation determined from the water or ice content of a cloud and described by Wilson and Ballard (1999);
- turbulent transport within the boundary layer as described by Lock et al. (2000) for the total specific humidity and by Roe (1985) for the cloud ice water content;
- convection based on the Gregory and Rowntree (1990) scheme;
- large-scale cloud as described by the new prognostic cloud scheme PC2 (Wilson et al. 2008);
- land surface processes calculated using MOSES (Cox et al. 1999).

Both observational and reanalysis data are used to evaluate the cloud and related variables from the climate simulation. The validation data used come from the ECMWF ERA15 (Gibson et al. 1997) and NCEP (Kalnay et al. 1996) reanalyses, ISCCP (Rossow and Schiffer 1991), ERBE (Harrison et al. 1990) and the Global Precipitation Climate Project (GPCP) (Huffman

et al. 1997) observational data products. The model output has been interpolated onto the same grid as the validation data (2.8 x 2.8 degrees) and monthly climatologies have been used in the following analysis.

Analysis of the AMIP simulation

The tropical (30N – 30S) circulation has been decomposed into 10 hPa/day bins and the resulting distributions for the reanalyses and the model simulation are plotted in Figure 1. The PDFs agree reasonably well, all showing negative skewness and a peak associated with the regimes of 10-20 hPa/day. The model has more occurrences than the reanalyses of strong ascent < -60 hPa/day and shows a greater peak in the dominant subsidence regimes. The magnitude of the pressure velocity associated with this peak corresponds to the clear-sky free tropospheric radiative cooling rate and reflects the large area of the tropical free troposphere that is cloudless (Bony et al. 2004).

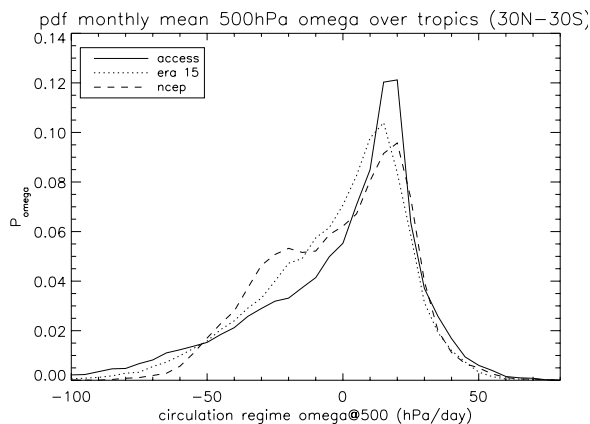


Figure 1. PDF of monthly mean omega at 500 hPa for ECMWF ERA15, and NCEP reanalyses and for the ACCESS AMIP simulation.

Using the analysis methodology of Bony et al. (2004), cloud and radiative fields are composited as a function of the circulation regime depicted in Figure 1. CRF is used as a measure of how clouds affect the radiation budget at the top of the atmosphere. CRF is calculated for shortwave (CRF_{SW}) and longwave (CRF_{LW}) radiation as the difference between the clear-sky and all-sky radiation. Figure 2 shows the result of compositing the CRF fields as a function of dynamical regime. The model underestimates the CRF for most regimes in the tropics. The CRF_{SW} is strongest for the deepest convection. This

cooling effect reduces in magnitude as the strength of the ascent regime reduces. The disagreement between the model and the ERBE observations composited as a function of pressure velocity from the reanalyses also reduces as the strength of the large-scale ascent decreases. Using the two reanalyses gives an indication of the uncertainty associated with the vertical velocity field.

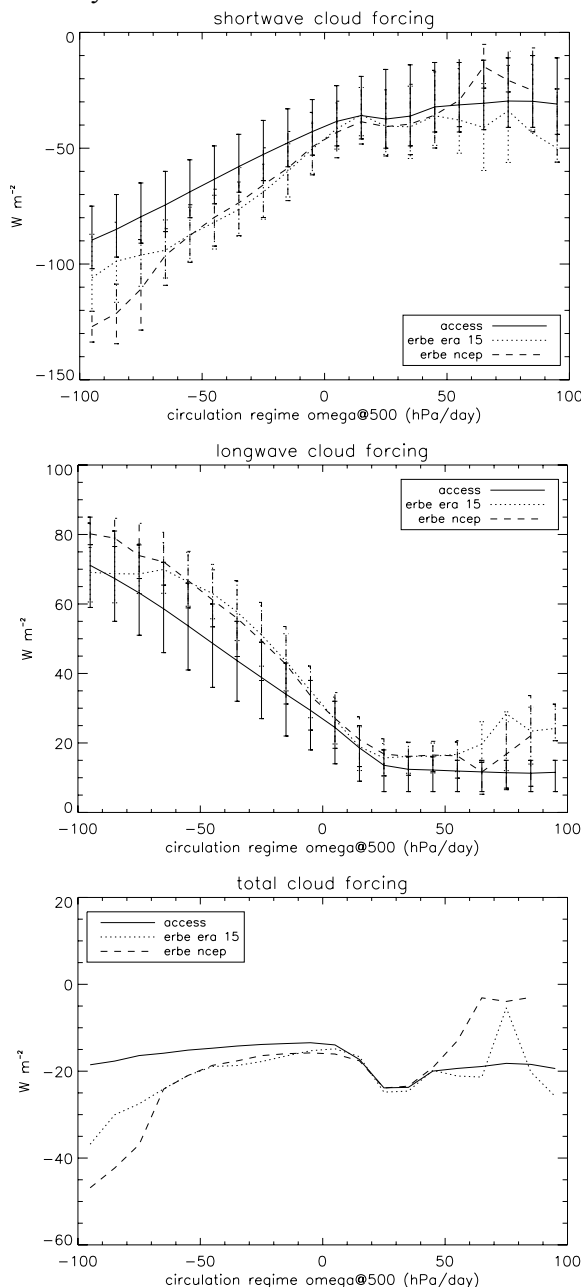


Figure 2. Shortwave, longwave and net cloud radiative forcing as a function of circulation regime. The bars represent the 25th and 75th percentiles.

The largest variability in CRF_{SW} , as shown by the bars indicating the 25th and 75th percentiles, occurs for the weak subsidence regimes. This is due to the occurrence of both shallow cumulus and stratocumulus clouds in these regimes and the result of those differing cloud properties on the CRF_{SW} . The variability of the CRF_{LW} , however, shows less variability across these regimes as the cloud top heights do not vary greatly. The largest spread in the longwave radiative effect of clouds occurs for the strong ascent regimes that produce convective clouds systems consisting of a wide array of cloud top heights.

The total CRF is the sum of the CRF_{SW} and CRF_{LW} and Figure 2 shows that the model underestimates the net cloud radiative forcing in the ascent regimes, predominately from the lack of shortwave cooling associated with cloudy skies. The net CRF in the weak subsidence regimes, which comprises the largest area of the tropics (see Figure 1), compares well with the ERBE observations and the stronger subsidence regimes show values that are within observational uncertainties. Note that the tails of the distribution have limited samples and, therefore, the statistical confidence of the comparison between the model and observations for these regimes is not high. While the model produces a comparatively good total CRF for the dominant subsidence regimes, it achieves this partly through cancellation of errors in the CRF_{SW} and CRF_{LW} .

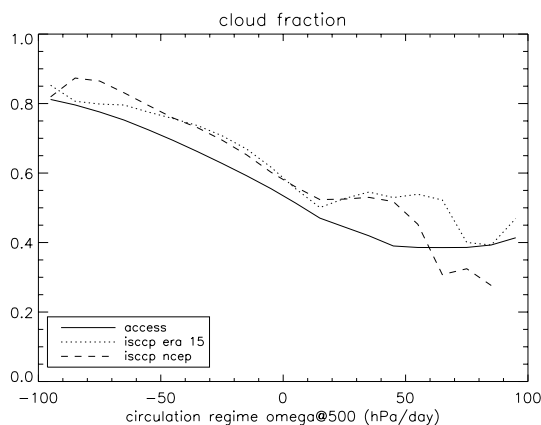


Figure 3. Total cloud fraction as a function of circulation regime.

Figure 3 shows that the cloud cover or fraction is underestimated in the model for all dynamical regimes in the tropics except for the tails of the

distribution. The largest underestimate occurs in the weaker subsidence regions where the cloud forcing compares well with observations. Together these results show that the model is simulating thicker clouds in these subsidence regimes than the observations in order to produce reasonable CRF fields.

To compare the state variables that the model simulates in the tropical dynamical regimes the temperature perturbation and relative humidity composites are shown in Figures 4 and 5.

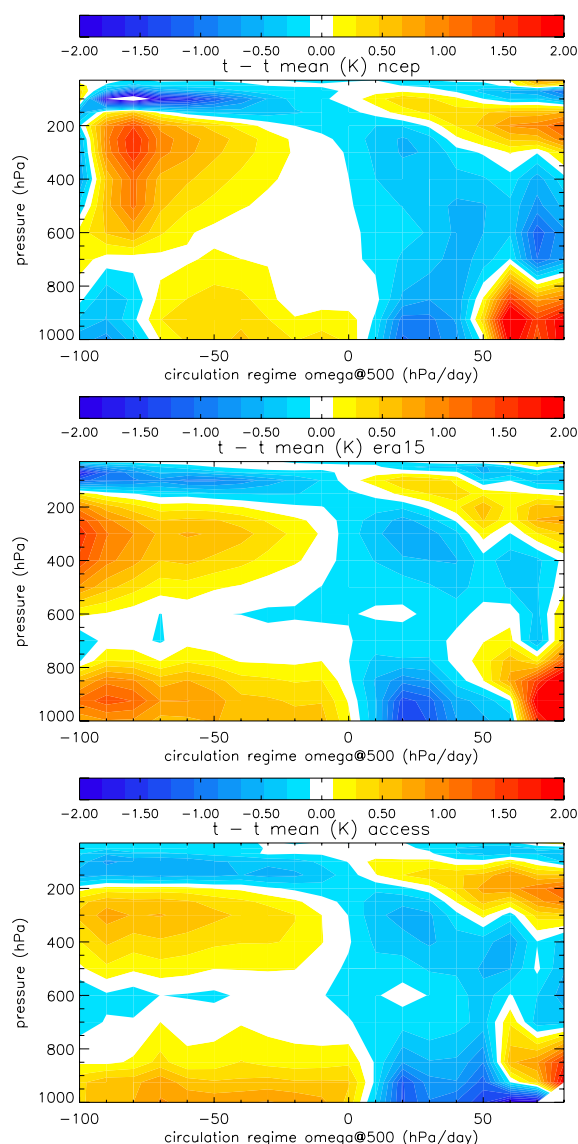


Figure 4. Temperature perturbation as a function of circulation regime.

The temperature perturbation, which is the perturbation taken from the zonal mean, shows vertically distributed warm perturbations in the ascent regimes of the model and reanalyses and cool perturbations in the subsidence regimes. The reverse is seen above 150 hPa in the reanalyses and 200 hPa in the model due to an elevated cooler tropopause over the ascent regions (Wyant et al. 2006). The weaker warm perturbations associated with the model convective regimes gives evidence that supports the CRF biases that the convective clouds are too thin with an incorrect distribution of heat, particularly in the upper regions of the deep clouds.

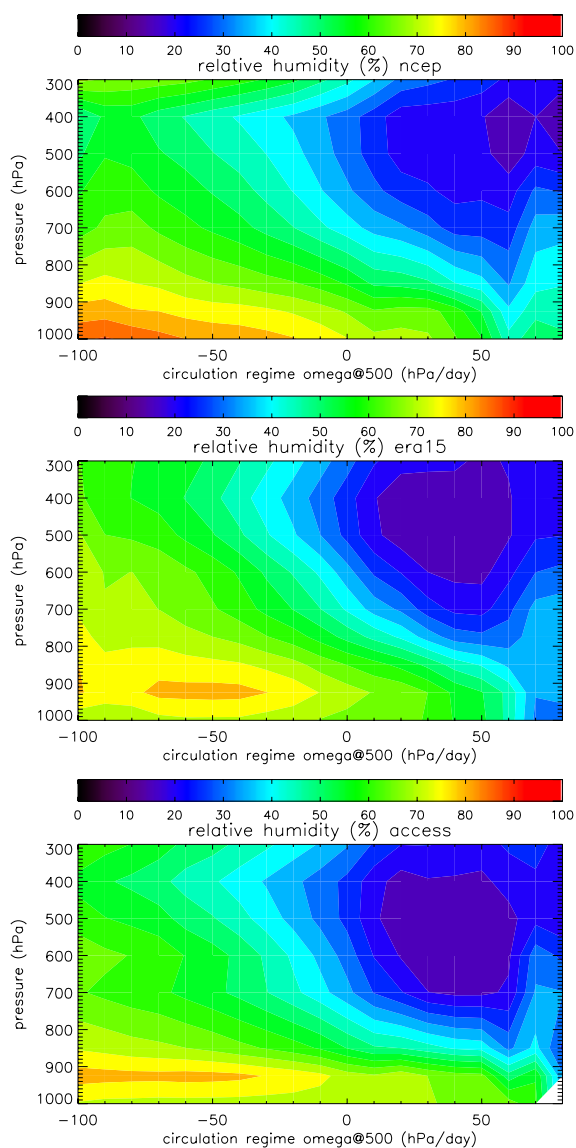


Figure 5. Relative humidity as a function of circulation regime.

The temperature perturbation profile in the subsidence regimes is very similar for the reanalyses and the model for the weaker pressure velocity magnitudes. However, for subsidence rates > 40 hPa/day, the model has a stronger cool perturbation, with the model maintaining a cool perturbation when the subsidence rate increases and the reanalyses show warm low-level anomalies. The relative humidity composites shown in Figure 5 reveal that the model water vapour distribution in the convective regions of the tropics has many similarities with those of the reanalyses. The relative humidity increases with height as the strength of the ascending motion increases, with all ascent regimes having high relative humidity in the boundary layer. There is a significant difference in the moisture of the low-levels in the subsidence regimes, with the model showing higher relative humidity than both of the reanalyses. The higher humidity in the model in these regions occurs in a shallower layer, with lower relative humidity values in the model at a given height above 850 hPa.

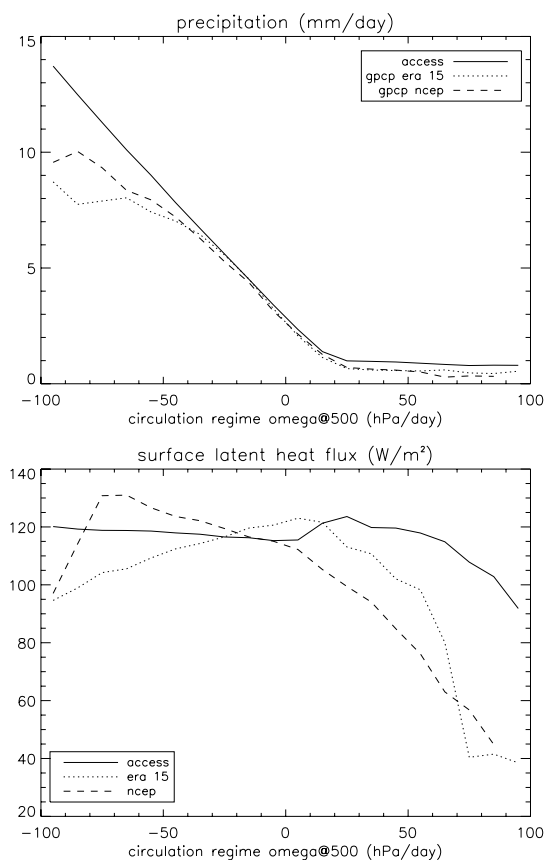


Figure 6. Precipitation and surface latent heat flux as a function of circulation regime.

There is significant disagreement between the reanalyses, particularly in the upper troposphere, indicating the large uncertainties and as such caution needs to be taken in drawing conclusions regarding the moisture distribution in the model using these data. To explore the reasons for the moist bias in the boundary layer of the subsidence regimes, the precipitation and surface latent heat flux are shown in Figure 6. The model produces greater precipitation for the convective regimes with 500 hPa ascent < -40 hPa/day and also for the subsidence regimes > 20 hPa/day. The over prediction of surface rain rate that the model produces compared to GPCP in these regimes is about 30%. This finding supports the result that was found from the CRF and cloud cover that the model produces thicker clouds in the subsidence regimes than the observations. These thicker clouds produce greater amounts of precipitation, enhanced evaporation in the subcloud layer (see Figure 6) and a moist bias in the boundary layer of these widespread subsidence regions in the tropics. However, it should be noted that there are significant uncertainties associated with the latent heat fluxes from the reanalyses, as can be seen from the differences shown in Figure 6, and therefore the necessary cautions need to be considered when comparing the model data with that from the reanalyses.

Conclusions

Analysing the ACCESS/UM AMIP simulation by regime sorting using mid-tropospheric velocity following Bony et al. (2004) has shown that the model underestimates the CRF_{sw} and CRF_{LW} for most of the dynamical regimes in the tropics as compared to the ERBE observations composited as a function of ERA15 and NCEP reanalyses pressure velocity. There is partial cancellation of these biases producing a reasonable net cloud forcing in all regimes except for the deepest convection. The weaker CRF_{sw} associated with these deep convective clouds and the greater precipitation suggest that the clouds are not thick enough. This could be due to the precipitation efficiency of the convection scheme being too high, removing too much cloud water as rain water resulting in thinner clouds. The dominant regime in the tropics is that with subsidence rates of 10-20 hPa/day. This regime in the model produces good agreement with reanalyses and observations for the CRF,

however, the cloud cover is about 30% lower than the ISCCP observations. This implies that these boundary layer clouds in the model are too thick, which was shown to result in an over prediction of precipitation, enhanced subcloud evaporation and a moist bias in the boundary layer when compared to the reanalyses.

Acknowledgements

Rob Colman is thanked for providing helpful comments on this note.

References

- Bony, S and coauthors, 2004: On dynamic and thermodynamic components of cloud changes. *Climate Dynamics*, **22**, 71-86.
- Cox, P and coauthors, 1999: The impact of new land surface physics on the GCM simulation of climate and climate sensitivity. *Clim. Dyn.*, **15**, 183-203.
- Davies, T. and coauthors, 2005: A new dynamical core for the Met Office's global and regional modeling of the atmosphere. *Q. J. R. Meteorol. Soc.*, **131**, 1759-1782.
- Edwards, J.M. and A. Slingo, 1996: Studies with a flexible new radiation code. I: Choosing a configuration for a large-scale model. *Q. J. R. Meteorol. Soc.*, **122**, 689-719.
- Gibson, R. and coauthors, 1997: *ECMWF Re-Analysis Project Report Series I*. ERA Description, ECMWF.
- Gregory, D. and P.R. Rowntree, 1990: A mass flux convection scheme with representation of cloud ensemble characteristics and stability-dependent closure. *Mon. Wea. Rev.*, **118**, 1483-1506.
- Harrison, E. and coauthors, 1990: Seasonal variation of cloud radiative forcing derived from the Earth Radiation Budget Experiment. *J. Geophys. Res.*, **95**, 18687-18703.
- Huffman, GJ and coauthors, 1997: The Global Precipitation Climatology Project (GPCP) combined precipitation dataset. *Bull. Amer. Met. Soc.*, **78**, 5-20.
- Kalnay, E. and coauthors, 1996: The NCEP/NCAR 40-year reanalysis project. *Bull. Amer. Met. Soc.*, **77**, 437-471.
- Lock, A. and coauthors, 2000: A new boundary layer mixing scheme. I: Scheme description and single-column model tests. *Mon. Wea. Rev.*, **128**, 3187-3199.
- Roe, P.L., 1985: Large-scale computations in fluid mechanics. *Lectures Appl. Math.*, **22**, 63.
- Rossow, W. and R. Schiffer, 1991: ISCCP cloud data products. *Bull. Amer. Met. Soc.*, **72**, 2-20.

Wilson, D. and S. Ballard, 1999: A microphysically based precipitation scheme for the Meteorological Office Unified Model. *Q. J. R. Meteorol. Soc.*, **125**, 1607-1636.

Wilson, D. and coauthors, 2008: PC2: A prognostic cloud fraction and condensation scheme. I: Scheme description. *Q. J. R. Meteorol. Soc.*, DOI:10.1002/qj.333.

Wyant, M. and coauthors, 2006: A comparison of low-latitude cloud properties and their response to climate change in three AGCMs sorted into regimes using mid-tropospheric velocity. *Climate Dynamics*, **27**, 261-279.

Simulating the atmospheric transport of CO₂ and SF₆ using the UK Met Office Unified Model

Rachel. M. Law^A and Katherine. D. Corbin^B

^{AB}Centre for Australian Weather and Climate Research

CSIRO Marine and Atmospheric Research

Rachel.Law@csiro.au

Introduction

Over recent decades, the ability to model atmospheric CO₂ has become important for a number of applications. ‘Top-down’ estimates of carbon fluxes use modelled atmospheric transport to invert atmospheric measurements of CO₂ (e.g. Gurney et al., 2002). Climate models often now include full carbon cycles to assess how warming may be accelerated by a positive feedback between carbon and climate (Friedlingstein et al., 2006); the atmospheric transport of CO₂ forms one component of the carbon cycle.

Most modelling studies used for atmospheric inversions of CO₂ and a few used for climate-carbon feedback studies have compared the simulated CO₂ transport through a series of ‘TransCom’ experiments. Early experiments focused on simple forward simulations with prescribed fluxes of fossil and biospheric CO₂ (Law et al., 1996) and SF₆ (Denning et al., 1999). A large body of work followed that assessed the sensitivity of CO₂ inversions to the transport model used (e.g. Gurney et al., 2002; Gurney et al., 2004; Baker et al., 2006). More recently a new set of forward simulations (TransCom-continuous or TC-cont) compared models on synoptic and diurnal timescales (Law et al., 2008 [L08]; Patra et al., 2008).

The Australian Community Climate and Earth System Simulator (ACCESS) is a coupled atmosphere ocean model with intended carbon cycle and chemistry capabilities. The atmospheric component of ACCESS is the UK Met Office Unified Model (UM), which has not previously been used for CO₂ inversion work, nor participated in any TransCom experiments. Here we report on some first tests of the UM model

using prescribed carbon and SF₆ fluxes from the most recent TransCom experiment. The aim was to understand the characteristics of CO₂ transport in the UM model before the existing land-surface module (MOSES) is replaced by CSIRO’s Community Atmosphere-Biosphere Land Exchange (CABLE) model.

Model simulations

The UM model has been run at 3.75° longitude by 2.5° latitude (N48) with 38 levels in an AMIP-style configuration. The simulations were started from January 1991 and integrated forward for 5 years. The first two years are excluded from the analysis as the tracer distribution spins up, and the results presented here use averages from the last three years. Five trace gases were simulated: biospheric CO₂ using CASA monthly mean and diurnally varying fluxes, ocean CO₂, fossil CO₂ and SF₆. The input flux fields are those used in the TC-cont experiment and are described in L08.

TC-cont required models to be driven by or nudged to analyses for 2000-2004, so that hourly trace gas timeseries could be compared to in-situ CO₂ observations for 2002 and 2003. In the UM simulations, the model is forced only with monthly mean sea surface temperatures and run for different years, so we are unable to compare the results at synoptic timescales. Instead we focus on diurnal timescales (as in L08) after a brief analysis of large-scale, annual mean and seasonal behaviour. Comparisons of large-scale tracer transport between models was not the aim of TC-cont and model output was submitted only at specified locations.

The UM model can be run in many different

configurations. Here we have tested the sensitivity of the CO₂ and SF₆ transport to the parameterization of the stable boundary-layer. Once the boundary-layer has been diagnosed as stable, mixing is parameterized using a local, first order mixing length closure scheme (Lock, 2007) where the turbulent diffusivities are a function of Richardson Number (R_i). There is a variety of choices for this function, and here we test three of them: (A) ‘Sharpest’ where $f(R_i)=(1-5R_i)^2$ for $0 < R_i < 0.1$ and $f(R_i)=(20R_i)^{-2}$ for $R_i > 0.1$, (B) ‘Long-tailed’ where $f(R_i)=1/(1+10R_i)$ and (C) a hybrid scheme which uses the sharpest function over the ocean and the long-tailed function over land. This hybrid scheme, C, has been suggested as best for NWP simulations, recent AMIP climate runs use function A, and the UM User Interface ‘help’ notes that B is the default option.

SF₆ inter-hemispheric difference

The principal source of SF₆ to the atmosphere is slow leakage primarily from electrical switching equipment, with no significant seasonal cycle in the emissions, with about 95% of the emissions in the northern hemisphere, and with no known atmospheric sources or sinks below 60 km. This makes it a useful indicator of model transport and inter-hemispheric mixing (e.g.; Denning et al., 1999; Peters et al., 2004; Patra et al., 2009). L08 fitted a spline to annual mean SF₆ at marine boundary-layer (MBL) sites to calculate the inter-hemispheric difference (IHD) for the global models that submitted results to TC-cont. They found a model mean IHD of 0.28 ± 0.07 ppt compared to 0.23 ppt for the observed SF₆ in 2002.

The annual mean IHD in all three UM simulations (A: 0.33, B: 0.31, C: 0.32 ppt) is larger than both the observed and the TC-cont model mean SF₆ IHD (Figure 1, top). Since only MBL sites are used, the IHD is similar for each boundary-layer scheme, with the sharpest scheme having a slightly larger north-south gradient.

In addition to overestimating the IHD, the UM model also overestimates the seasonal cycle of the SF₆ IHD compared to TC-cont and observations; however, all UM cases capture the timing of the seasonal cycle seen in the majority of the TC-cont models and in the observations, with the greatest difference in March-May and the smallest differences in July-September (Fig 1,

bottom). The larger IHD suggests that the UM may not have enough inter-hemispheric mixing, and using the long-tailed scheme helps to reduce the IHD. Other transport processes will also impact inter-hemispheric mixing. Future tests may be required to test the sensitivity of the unstable boundary layer parameterization or of convection.

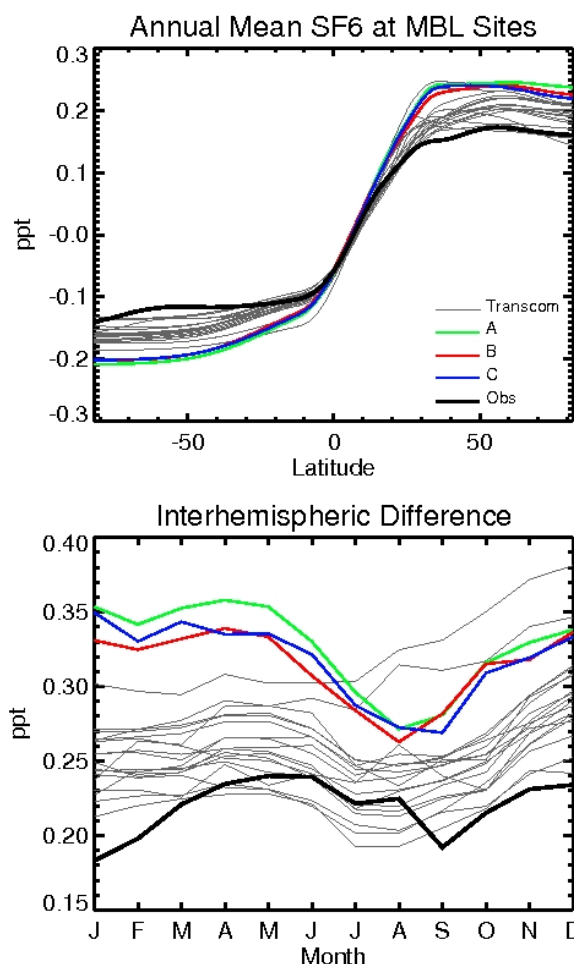


Figure 1. (Top) Spline fit to the annual mean SF₆ concentrations at MBL sites. The global mean concentration has been removed from all cases. The two TC models outside the one standard deviation range in L08 are not plotted here. (Bottom) Seasonal cycle of the IHD in SF₆, calculated by subtracting monthly hemispheric concentrations using a spline fit to the MBL sites. It should be noted that the monthly observations are highly sensitive to site selection due to the small number of samples per month.

CO₂ seasonal cycle

CO₂ observations (GLOBALVIEW-CO₂, 2007) show a large seasonal cycle in northern mid and

high latitudes due to a net biospheric CO₂ source in winter from respiration and net CO₂ uptake in summer due to photosynthesis. The seasonal signal is advected from the continent to MBL sites. In L08 the modelled and observed peak-to-peak (ptp) amplitudes (maximum minus minimum monthly concentration) were compared for MBL sites from 45-90°N. The modelled ptp amplitude using the CASA diurnally varying fluxes (12.8±2.0 ppm) was slightly lower than observed (14.2 ppm). The observations used are mainly flask records with day-time samples. For continental sites (and less significantly at marine sites) this would give lower concentrations during summer than if the full diurnal cycle was observed, leading to some amplification of the ptp amplitude. The impact of the diurnal cycle can be seen if the modelled ptp amplitude is calculated from the TC-cont simulations using monthly mean CASA fluxes instead of the diurnally varying ones. The modelled amplitude (13.5±2.3 ppm) is closer to the observed value.

The ptp amplitudes calculated from the UM simulations (Table 1) are similar to other models (and the observed amplitude) for the monthly mean CASA fluxes, but generally lower than other models when the CASA diurnal fluxes are used. Scheme A gives larger amplitudes than B or C, with larger differences for the case with monthly fluxes than with the diurnal ones. The large differences (2.3-3.7 ppm) when using the different fluxes is surprising given that the calculation is for MBL sites. Only one TC-cont model gives a difference as large. Unexpectedly, the major contribution to the difference is from the simulated concentration in winter rather than summer (when diurnal cycles are larger). This unusual result warrants further investigation.

Table 1. Average peak-to-peak amplitude (ppm) of the seasonal cycle of CO₂ for MBL sites between 45-90°N with different boundary-layer schemes and using CASA diurnal or monthly fluxes.

	CASA diurnal	CASA monthly
A	10.96	14.63
B	10.55	12.85
C	10.44	13.12

CO₂ diurnal cycle

Photosynthesis requires sunlight while respiration

does not. Consequently the biosphere is a source of CO₂ to the atmosphere at night and a sink of CO₂ during the day. This diurnal cycle of fluxes combined with diurnal variations in atmospheric mixing leads to significant diurnal cycles in atmospheric CO₂ at continental locations.

The UM model is run with a half-hourly timestep, and half-hourly tracer concentrations have been output for 79 grid-points where continuous CO₂ measurements are available. Here we analyse the summed concentration from the CASA diurnal, fossil and ocean fluxes. We have calculated average June-August (JJA) diurnal cycles at continental sites with continuous observations for 2002, and plot the peak-to-peak amplitude of the diurnal cycle following L08. Fig 2 shows the median and range of model results from L08, observed amplitudes and the UM results (not available for some sites).

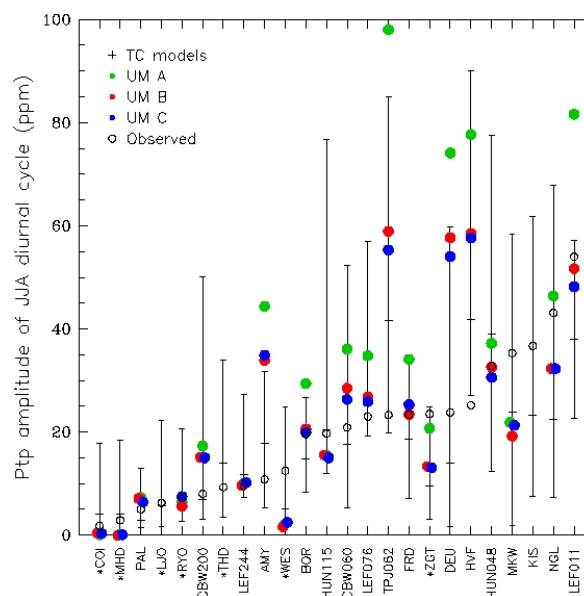


Figure 2. Peak-to-peak amplitude of the mean JJA diurnal cycle for observed 2002 CO₂ (open circle), TC-cont models for 2002 (error bar shows minimum, maximum and median model) and UM cases using scheme A (green dot), B (red dot), C (blue dot). The model amplitudes are calculated from the sum of concentrations from CASA diurnal, fossil and ocean emissions. Sites are listed on the x-axis and their locations are given in Table 2. CBW, LEF, HUN and TPJ are sampled at various vertical levels, which are specified in m. The asterisk indicates coastal sites.

Overall the modelled amplitudes increase as the

observed amplitudes increase. The large model spread/scatter in part reflects the limitations of representing an observing location with a model grid-point, especially for coastal sites. For example, the high modelled amplitudes at AMY, DEU and HVF are in part due to the fossil tracer contributing 25-30% of the diurnal amplitude whereas in reality these sites do not have significant local fossil emissions. Some differences from the observations (e.g. at TPJ) also occur because of the uncertainty in vertical sampling, i.e. which model level best represents a given observing height. We will illustrate this later.

Scheme A often gives larger amplitudes than the other two schemes, and these larger amplitudes are mostly a worse fit to the observations. This is seen by fitting a line to the observed and modelled amplitudes. For scheme A the slope of the line is 1.36 ($R^2=0.40$) compared to slopes of 0.90 ($R^2=0.40$) and 0.85 ($R^2=0.40$) for B and C respectively. L08 models gave slopes of 0.24-1.40 (median 0.62) with R^2 ranging from 0.17-0.60 (median 0.42).

Table 2. Latitude, longitude and reference for the CO₂ observation sites used in Figure 2.

Site	Lat	Lon	Reference
AMY	36.53	126.32	Kim and Park (2006)
BOR	55.87	-98.46	Dunn et al. (2007)
CBW	52.00	4.90	A. Vermeulen (pers. comm., 2006)
COI	43.15	145.50	Tohjima et al. (2006)
DEU	49.77	7.05	Uhse and Meinhardt (2006)
FRD	49.88	-81.57	Higuchi et al. (2003)
HVF	42.53	-72.17	Urbanski et al. (2007)
HUN	46.95	16.65	Haszpra (2006)
KIS	36.08	139.55	Muto (2006)
LJO	32.90	-117.30	R. Keeling (pers. comm., 2006)
MHD	53.33	-9.90	Biraud et al. (2002)
MKW	34.85	137.43	Iwata (2006)
NGL	53.15	13.03	Uhse and Meinhardt (2006)
PAL	67.97	24.12	Hatakka (2006)
LEF	45.93	-90.27	Bakwin et al. (1998)
RYO	39.03	141.83	Sasaki (2006)
TPJ	-2.86	-54.96	Hutyra et al. (2007)
THD	41.05	-124.15	Lueker et al. (2003)
WES	55.00	8.00	Uhse and Meinhardt (2006)
ZGT	54.43	12.73	Uhse and Meinhardt (2006)

CO₂ is measured continuously at a number of tall towers. Figure 3 shows the observed and modelled JJA diurnal amplitude at three northern mid-latitude towers (CBW, LEF, HUN) and one tropical tower (TPJ). Note that the amplitudes at TPJ (c) have been reduced by a factor of 3 to fit the plotted x-range. As we would expect, the diurnal amplitude decreases with height at all sites and in both the observations and the model simulations. Mostly the modelled amplitudes are larger than those observed, with schemes B and C generally being closer to the observations. Differences in diurnal amplitude persist above the first model level.

The TPJ observations (a Brazilian forest site) show a large increase in diurnal amplitude from 29 ppm at 39 m to 111 ppm at 20 m. This type of structure is clearly not resolved by the model with levels at 20 and 80 m and it is difficult to say which boundary-layer scheme would better represent the observations. In Fig 2, the model overestimate for TPJ is due to comparing the lowest model level with the 62 m level for the observations, rather than a lower observed level.

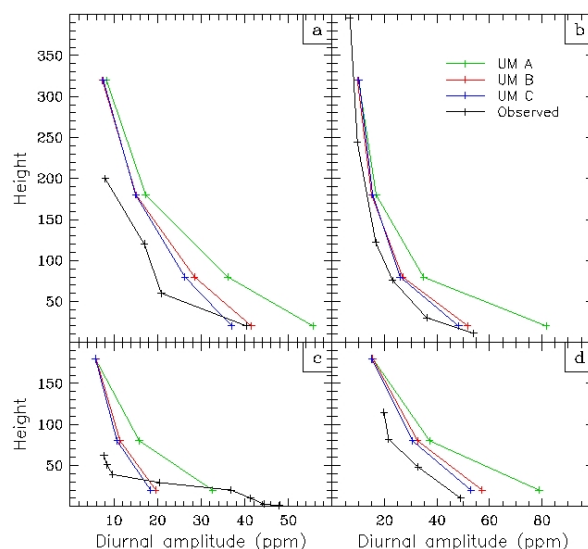


Figure 3. Ptp amplitude of the mean JJA diurnal cycle with height at CBW (a), LEF (b), TPJ (c) and HUN (d), for observed (black) and modelled CO₂ using scheme A (green), B (red) and C (blue).

To investigate the vertical mixing strength following L08, the ratio of the diurnal peak-to-peak amplitude concentration to the flux amplitude is calculated at seven continental, low-altitude sites (Figure 4). Here we used only the

CASA-diurnal modelled CO₂ and fluxes. The majority of the models and observations have ratios of 1-3 ppm/μmol.m⁻².s⁻¹, with the largest ratios at the TPJ and HUN sites. The UM scheme A has considerably higher ratios than schemes B and C, most TC-cont models, and the observations. The high ratios for scheme A suggest that the sharpest scheme underestimates the vertical mixing, and using the long-tailed or hybrid scheme more closely matches both the observations and the TC-cont mean.

Conclusions

The SF₆ simulation suggests that inter-hemispheric mixing is slower in the UM model (at N48 resolution) than for other models while the seasonal behaviour of CO₂ is broadly consistent with other models. The analysis at MBL sites shows little sensitivity to the choice of stable boundary-layer scheme. By contrast CO₂ diurnal cycles at continental sites can be very sensitive to the scheme chosen, with the sharpest scheme (A) generally giving larger amplitudes than the long-tailed (B) and hybrid (C) schemes and a worse comparison with observations. The next steps will be to assess whether the transport is similar at higher horizontal resolution (N96) and with the change in land surface scheme to CABLE.

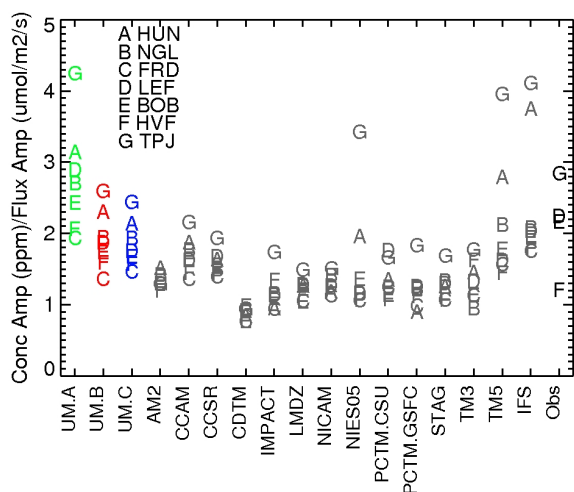


Figure 4. Ratio of peak-to-peak mean JJA diurnal concentration amplitude to diurnal JJA flux amplitude, using CASA diurnally varying tracer and flux for the models. Each site is indicated by a letter identified in the key, with the model listed along the x-axis. Observations are only currently available at LEF, BOB, HVF, and TPJ.

Acknowledgements

The TransCom-continuous model simulations were provided by AM2/AM2t (S. Fan, S.-J. Lin), CCAM (R. M. Law), CCSR_NIES (P. Patra, M. Takigawa), CDTM (T. Maki), CHIMERE (C. Aulagnier, L. Rivier, R. Vautard), COMET (G. Pieterse, A. T. Vermeulen), DEHM (C. Geels, J. Brandt, J. H. Christensen), IFS (S. Serrar), IMPACT (D. J. Bergmann, P. J. Cameron-Smith), LMDZ/LMDZ_THERM (P. Bousquet, F. Delage), NICAM (Y. Niwa, R. Imasu, M. Satoh), NIES05 (S. Maksyutov, R. Onishi), PCTM.CSU (R. Lokupitiya, A. S. Denning, N. Parazoo, J. Kleist), PCTM.GSFC (S. R. Kawa, Z. Zhu), REMO (U. Karstens), STAG/STAGN (S. Taguchi), TM3_fg/TM3_vfg (C. Rödenbeck), TM5_glb3x2/TM5_nam1x1 (W. Peters, L. Bruhwiler), TM5_eur1x1 (M. C. Krol, S. Houweling).

References

Baker, D. F., et al., 2006: TransCom 3 inversion intercomparison: Impact of transport model errors on the interannual variability of regional CO₂ fluxes, 1988–2003, *Global Biogeochem. Cycles*, 20(1), GB1002, doi:10.1029/2004GB002439.

Bakwin, P. S., P. P. Tans, D. F. Hurst, and C. Zhao, 1998: Measurements of carbon dioxide on very tall towers: Results of the NOAA/CMDL program, *Tellus, Ser. B*, 50, 401–415.

Biraud, S., P. Ciais, M. Ramonet, P. Simmonds, V. Kazan, P. Monfray, S. O’Doherty, G. Spain, and S. G. Jennings, 2002: Quantification of carbon dioxide, methane, nitrous oxide and chloroform emissions over Ireland from atmospheric observations at Mace Head, *Tellus, Ser. B*, 54, 41–60.

Denning, A.S., et al., 1999: Three-Dimensional Transport and Concentration of SF₆: A Model Intercomparison Study (TransCom 2). *Tellus*, 51B, 266-297.

Dunn, A. L., C. C. Barford, S. C. Wofsy, M. L. Goulden, and B. C. Daube, 2007: A long-term record of carbon exchange in a boreal black spruce forest: Means, responses to interannual variability, and decadal trends, *Global Change Biol.*, 13, 577–590, doi:10.1111/j.1365-2486.2006.01221.x.

Friedlingstein, P. et al., 2006; Climate-Carbon Cycle Feedback Analysis: Results from the C⁴MIP Model Intercomparison. *J. Climate*, 19, 3337-3353.

GLOBALVIEW-CO₂. 2007: Cooperative Atmospheric Data Integration Project - Carbon Dioxide. CD-ROM, NOAA CMDL, Boulder, Colorado. [Also

available on Internet via anonymous FTP to <ftp.cmdl.noaa.gov>, Path: [ccg/co2/GLOBALVIEW](ftp://ftp.cmdl.noaa.gov/ccg/co2/GLOBALVIEW)].

Gurney, K.R., et al., 2002: Towards robust regional estimates of CO₂ sources and sinks using atmospheric transport models. *Nature*, 415, 626-630.

Gurney, K.R., et al., 2004: Transcom 3 inversion intercomparison: Model mean results for the estimation of seasonal carbon sources and sinks. *Global Biogeochem. Cycles*, 18, GB1010, doi:10.1029/2003GB002111.

Haszpra, L., 2006: Atmospheric CO₂ hourly concentration data, Hegyhatsal, in World Data Centre for Greenhouse Gases, Japan Meteorol. Agency, Tokyo. (Available at <http://gaw.kishou.go.jp/wdcgg.html>)

Hatakka, J., 2006: Atmospheric CO₂ hourly concentration data, Pallas, in World Data Centre for Greenhouse Gases, Japan Meteorol. Agency, Tokyo. (Available at <http://gaw.kishou.go.jp/wdcgg.html>)

Higuchi, K., D. E. J. Worthy, D. Chan, and A. Shashkov, 2003: Regional source/sink impact on the diurnal, seasonal and inter-annual variations in atmospheric CO₂ at a boreal forest site in Canada, *Tellus, Ser. B*, 55, 115–125.

Hutyra, L., J. W. Munger, S. R. Saleska, E. W. Gottlieb, B. C. Daube, A. L. Dunn, D. F. Amaral, P. B. de Camargo, and S. C. Wofsy, 2007: Seasonal controls on the exchange of carbon and water in an Amazonian rainforest, *J. Geophys. Res.*, 112, G03008, doi:10.1029/2006JG000365.

Iwata, S., 2006: Atmospheric CO₂ hourly concentration data, Mikawa-Ichinomiya, in World Data Centre for Greenhouse Gases, Japan Meteorol. Agency, Tokyo. (Available at <http://gaw.kishou.go.jp/wdcgg.html>).

Kim, J.-S., and K.-J. Park, 2006: Atmospheric CO₂ hourly concentration data, Anmyeon-do, in World Data Centre for Greenhouse Gases, Japan Meteorol. Agency, Tokyo. (Available at <http://gaw.kishou.go.jp/wdcgg.html>)

Law, R.M., et al., 1996: Variations in modelled atmospheric transport of carbon dioxide and the consequences for CO₂ inversions. *Global Biogeochem. Cycles*, 10, 783-796.

Law, R. M., et al., 2008: TransCom model simulations of hourly atmospheric CO₂: Experimental overview and diurnal cycle results for 2002, *Global Biogeochem. Cycles*, 22, GB3009, doi:10.1029/2007GB003050

Lock, A., 2007: The parametrization of boundary layer processes, UM version 6.3, Documentation paper No 24.

Lueker, T. J., S. J. Walker, M. K. Vollmer, R. F. Keeling, C. D. Nevison, R. F. Weiss, and H. E. Garcia, 2003: Coastal upwelling air-sea fluxes revealed in atmospheric observations of O₂/N₂, CO₂ and N₂O, *Geophys. Res. Lett.*, 30(6), 1292, doi:10.1029/2002GL016615.

Muto, Y., 2006: Atmospheric CO₂ hourly concentration data, Kisai, Mt. Dodaira, in World Data Centre for Greenhouse Gases, Japan Meteorol. Agency, Tokyo. (Available at <http://gaw.kishou.go.jp/wdcgg.html>)

Patra, P. K., et al., 2008: TransCom model simulations of hourly atmospheric CO₂: Analysis of synoptic-scale variations for the period 2002–2003, *Global Biogeochem. Cycles*, 22, GB4013, doi:10.1029/2007GB003081.

Patra, P. K., et al., 2009: Transport mechanisms for synoptic, seasonal and interannual SF₆ variations and “age” of air in troposphere, *Atmos. Chem. Phys.*, 9, 1209-1225.

Peters, W., et al., 2004: Toward regional-scale modeling using the two-way nested global model TM5: Characterization of transport using SF₆, *J. Geophys. Res.*, 109, D19314, doi:10.1029/2004JD005020.

Sasaki, H., 2006: Atmospheric CO₂ hourly concentration data, Ryori, in World Data Centre for Greenhouse Gases, Japan Meteorol. Agency, Tokyo. (Available at <http://gaw.kishou.go.jp/wdcgg.html>).

Tohjima, Y., H. Mukai, T. Machida, Y. Fujinuma, and M. Katsumoto, 2006: Atmospheric CO₂ hourly concentration data, Cape Ochi-ishi, in World Data Centre for Greenhouse Gases, Japan Meteorol. Agency, Tokyo. (Available at <http://gaw.kishou.go.jp/wdcgg.html>)

Uhse, K., and F. Meinhardt, 2006: Atmospheric CO₂ hourly concentration data, Deuselbach, Neuglobsow, Schauinsland, Westerland, Zingst, Zugspitze/Schneefernerhaus, in World Data Centre for Greenhouse Gases, Japan Meteorol. Agency, Tokyo. (Available at <http://gaw.kishou.go.jp/wdcgg.html>)

Urbanski, S., et al. 2007: Factors controlling CO₂ exchange on timescales from hourly to decadal at Harvard Forest, *J. Geophys. Res.*, 112, G02020, doi:10.1029/2006JG000293.

Introducing the Natural Language Generation of Text Weather Forecasts in the GFE

Tennessee Leeuwenburg

Centre for Australian Weather and Climate Research

Bureau of Meteorology

t.leeuwenburg@bom.gov.au

Introduction

The text formatters in the Graphical Forecast Editor (GFE) bring together the two disciplines of computational linguistics and weather science. The formatters are software modules, capable of pursuing goal-directed behaviour to generate English-language weather forecasts in a similar style to that used by weather forecasters in live operations.

Whereas much scientific research concentrates on the supply of good numerical forecast guidance, the work involved in producing text formatters concerns itself with how to represent the most important aspects of that guidance as text to end-users. Conveying the correct meaning in a piece of text can be critical to life (as in the case of warning forecasts). The text formatters must guarantee the full reporting of that information, in addition to being assessed according to the clarity and elegance of the forecast.

Computer users will be aware of how rigid any automated system can be. The text formatters have a complex engine driving them, which allows for high-level, language-directed goals to be captured. There are two vectors of work involved in producing excellent weather forecast text. The first relates to work on the fundamental capabilities of the text formatters. The second relates to configuring and specialising that fundamental capacity so that it delivers reports which are in line with the requirements of various stakeholder groups.

The formatters provide the means by which scientific rigor in weather description can be maintained. For the first time it is possible to be clear about exactly what conditions will trigger a warning condition, in a way which relates directly

to the underlying guidance data. Removing the human from first-guess forecast generation means that precise meaning can be attached to the words used, rather than relying on the analogy or mental construct of the weather situation to arrive at the resulting description.

A Short Introduction to the GFE

Development of the GFE began in 1992 by the USA National Weather Service, first producing a full suite of digital products in 2003 (LeFebvre, Mathewson and Hansen 2003). It is operationally deployed across the USA, producing both graphical and text-based forecasts.

The GFE is made up of a graphical client and a data server, with the bulk of the functionality being initiated by a human forecaster. The client allows forecasters to not only view, but directly manipulate, NWP forecast guidance, other forecast guidance systems and observational and analysis data.

One major shift with the introduction of the GFE is that text and graphical forecast production systems are almost fully automated. The main work of the forecaster is producing a modified set of forecast data grids. If this were done in a fully ad-hoc way, the potential would exist for these grids to become quite implausible in physical terms. Unlike NWP modeling, conservation of energy and parameter consistency is not maintained, nor is it feasible to do so.

However, in order that grid manipulations (a) are reasonably easy to perform, (b) operate in a scientifically defensible manner to the extent possible and (c) support the range of operations required to create a set of forecast grids,

automated tools known as Smart Tools have been developed. The first Australian set of these, representing years of effort from CAWCR and NOAA, are a launching pad for further research and development. They open up avenues for research into algorithmic post-NWP mechanisms, such as capturing topographic effects and deriving weather parameters which are not explicitly modeled.

Once a set of forecast grids is thus produced, the forecast product generation is highly automated. (While graphical forecast products may be generated, the current research focus is on text forecasts.)

The text formatters, which do this work, operate with four components of evaluation:

1. Statistical sampling and data representation
2. Information processing
3. Language representation
4. Post-processing

These stages may be considered sequentially, but there is always feedback between the components when actually producing forecasts.

Work on the text formatters, then, falls into a variety of areas:

1. Algorithms and techniques in language processing
2. Studies into the effective use of language generally (such as appropriate grammar, choosing a good lexicon of terms, understanding what makes a sentence clear and comprehensible)
3. An examination of how forecasters choose to express concepts regarding future conditions, both to mimic this and also to identify any surmountable communication difficulties.
4. The gathering of requirements from a services perspective relating to what must be guaranteed when a forecast is produced (for example, the guarantee that forecast text will always mention peak wind speeds during warning conditions, or that District forecasts will always include thunderstorms if they are forecast for more than 5% of the area).
5. Ensuring that terminology is used in a consistent fashion (quantification of forecast terms used).

6. Expansion of the expressions used to incorporate probabilistic guidance and new forms of forecast.

This work involves a variety of tasks, varying from fundamental research, to engineering and information management. The algorithms and theories that describe how to go about information processing and language representation are the focus of much on-going academic activity. Unlike physical science, this is often less mathematical and more concept- or design-based. It is a less mature area of research and can involve much searching in the dark.

The examination of forecast terminology and consistency between forecasts has not previously had a large amount of resource directed towards it, partially due to the human factors involved. While there is a call for greater consistency of terminology, it has become clear during the GFE implementation that not all concepts of 'consistent' are equally applicable. The statistics which make a forecast term appear in one product but not another (e.g. a Town versus a District) can result in the appearance of inconsistency between written forecasts, even when the underlying rules are being applied in a consistent fashion. Negotiating the relationship between the rules which define the system and the requirements which are placed on the output of the system is too much a matter of experience and intuition.

The tacit knowledge held by a human forecaster is something which needs to be drawn out and considered, rather than a source of consistent advice regarding the appropriate behaviours to attempt to build in to the automated system.

While the drivers for GFE development are currently coming strongly from the IT discipline (that is, being driven by bug reports and feature requests) rather than science (verification results, experimentation and evaluation), it is expected that with the national rollout, and with increased certainty in the future of the GFE, that progress in the fundamental capabilities of the text generation system will come from applying research techniques as much by ad-hoc problem-solving. Getting the most from the partnership with NOAA will also be important.

Text Generation and Computational Linguistics

There are a number of key papers within the domain of Computational Linguistics which are useful for placing the GFE text formatters into academic context. One such paper is presented by De Smetd et al., (1996). This impeccably-researched paper critically analyses a number of existing Natural-Language Generation (NLG) systems and sketches some new directions for further research. In their language, the GFE formatters exhibit features of both interactive (feedback) systems, blackboard systems and revision-based systems. These architectural types refer to the way in which the relevant systems proceed through two well-recognised stages: text or document planning and surface realization or lexicalization – or in layman's terms, what to say and how to say it (p3).

As acknowledged, these stages are not entirely independent. What you want to communicate is influenced by what you are able to say. Some concepts are remarkably hard to describe, while others can be expressed in just a few words. De Smetd, Horacek and Zock also state that few existing systems are really very capable:

“In the area of text planning, researchers have identified more problems and limitations of existing theories than they have provided new solutions. With regard to lexicalisation, only a few researchers have made proposals that go beyond one-to-one mappings between concepts and words...”

The GFE formatters have a number of features which place them at the more complex, more sophisticated end of the spectrum. In other respects, they are probably a little behind the game. Where they excel is in document planning and the way in which document planning and lexicalization dynamically interact with one another. In terms of shortcomings, more work is necessary to extend the number of grammatical constructs they can support. It needs to be easier to quickly implement new phrases.

A fertile area for new research is partial specification. Frequently, systems are put together without a distinction between must-goals and should-goals. An example of a must-goal would be to always mention the timing of when wind speeds increase past a warning threshold. An example of a should-goal is to describe wind

changes in 5-knot increments, but this may come second to other should-goals relating to ideal sentence length.

The GFE has no inherent concept of a must-goal in terms of explicitly listing and separating the two goal types. Indeed, there is no explicit separation of goal-directed and rule-based processing components. However, both goal-directed behaviour and dynamic goal conditions have been implemented into the basic structure of the formatters.

It is also enlightening to compare the GFE text formatters to its close cousins. SumTime-Mousam (STM) is an NLG system for wind forecasts (Reiter et al., 2005). Further, Reiter is one of only a few authors to include a proper evaluation of the relative performance of the automatically-produced text as compared with human-authored text. Information on the entire scope and capability of the system is limited, with the research reports and available web information concentrating only on the wind-phrase generation logic. FOG is another NLG system for Atlantic Marine forecasts by the Atmospheric Environment Service of Environment Canada (Goldberg, et al., 1994).

The research findings are very much relevant to the development of the GFE formatters, both in terms of the computer science aspects and in terms of the lexicon-design and requirements-negotiation processes. We will first look at the implications for system design, before addressing issues of word choice and requirements later in this article.

STM is less complex in many respects than the GFE formatters, but with some particular advantages over the GFE formatters in terms of an expanded lexicon of verb terms (which it uses particularly effectively). The key difference between the two systems is the capacity of the GFE to react to the complexity of the meteorological situation and adjust its should-goals appropriately.

STM will seek to represent every detail of the situation entered as a data input, potentially resulting in an overly-lengthy phrase. To combat this, STM also employs the use of acronyms to describe compass-point directions. By contrast, the GFE formatters have to include a great deal of situation-recognition logic in order to distil from

raw statistics what is significant about a weather situation and how to summarise that effectively while still communicating the salient points. STM appears to have a two-level detail response capacity, whereas the GFE has up to eight levels of detail with independent settings for strong or light prevailing conditions.

Architecturally, STM appears to explicitly represent various NLG stages: document planning, microplanning (lexicalization) and aggregation. Aggregation is used in the STM research to mean the distillation of information among sentences.

Compared with STM, the GFE formatters have greater responsibility for distilling information from raw statistics and more capacity to capture high-level goals, but have a slightly less capable lexicalization system as currently deployed. (That is to say, it is not so much the system which is limited, as the number of words currently used to describe changes in conditions.)

Text Generation and Meteorology

The main links between text generation and meteorology are data processing and information representation. To date, the key performance indicator of the GFE has been the verification results of forecast data grids produced by the system. Examples of such work include Stern (2007). In terms of general, written-forecast metrics, available research concentrates on the statistical accuracy of the forecasts rather than on the semantic clarity of the forecasts (Toth et al., 2006).

It is believed that this is in large part due to the lack of a clear quantitative method for assessing the semantic clarity of a piece of written text. As such, assessment has taken the form of qualitative analysis, survey results and intuitive response.

All of this makes verification statistics of text forecasts extremely hard and expensive to produce. Evaluation is a painstaking manual process. It is possible to glimpse how more objective metrics of forecast text might be derived, such as performing an analysis of grammatical complexity, but such things are not achievable now.

Further, the quantitative analysis of operational forecasts has tended to be used for post-

development, forecaster evaluation. That is to say, the verification of guidance systems has been “over here”, while the analysis of forecaster performance has been “over there”.

The challenge, then, is to discover the links between meteorology and text generation, and what each discipline can learn from the other.

The text formatters, as a means of mechanically producing text forecasts (potentially from raw model guidance), significantly narrow the distance from here to there. In so doing, they provide meteorological researchers with the means to much more quickly influence the worded text forecasts.

One example of this in the GFE is the use of probabilistic information. While the GFE currently only makes use of such information as input into derived weather grids (which store non-probabilistic coverages such as “scattered”), this is likely to change. As more probabilistic guidance becomes available through ensemble modeling, the capacity exists to very quickly reflect that additional information in the forecast words. Previously, such a change would have required significant forecaster training.

This potentially brings in a much closer connection between forecast expression and meteorological knowledge. Scientists who are working on novel systems have the potential to have a role in determining how their information could be integrated into the final forecast products. Information also flows the other way – gaps in what can be described in the text forecasts could potentially highlight gaps in the guidance systems.

Word Choice and Expression

It is the issue of word choice and grammar which have dominated discussions when building the formatters in the GFE. I used to describe these issues as being moving the tip of an iceberg. Changing the words also involves change to a large, hidden body of Python code which does not move as fast as new expressions can be imagined. Another, equally valid metaphor is that of genotype and phenotype. The requirements are all on the phenotype: what the forecasts should look like, while the work is all on the genotype: how the formatters are coded and configured. There is an enormous amount of semantic awareness held

by both researchers and forecasters alike, much of which is consciously accessible, and much of which is only tacit.

This introduces several complicating factors, not the least of which is the time-consuming process of talking to people about their tacit knowledge, in order to try to systematize and capture that knowledge. The major issues are essentially due to (a) the unforeseeability of exactly what new language will emerge from implementing a new rule, and (b) differences between important stakeholder groups regarding what is the appropriate way to describe a given weather situation.

Before the advent of the GFE, individual differences were accommodated by simply allowing small differences to be reflected in the official forecasts – indeed those differences would often pass entirely unnoticed. It was not just possible, but actually the case, that one forecaster might use a term such as “chance” to describe a situation, where the next person would use “isolated”. The problems were more serious when individual instincts regarding whether conditions were serious enough to warrant issuing a warning came into play.

Nobody questions whether forecasters act with skill or to the best of their ability, but individual differences were generally not forced into alignment. Further, forecasters were given little opportunity to learn whether their forecasts were resonating with the public or not. Such feedback as was available came as the result of intermittent, ad-hoc and unfocussed feedback surveys rather than being an ongoing part of their jobs.

These differences of opinion are also reflected in some ways within the individuals involved in setting direction and policy. Every person involved in the GFE text formatter process, including the developers, managers, reviewers and forecasters has taken part in a discussion about what is the best way to talk to the public about the weather. The gulf between a naïve understanding of the weather and a meteorologist’s understanding of the weather is sometimes very large.

For better or for worse, the GFE formatters support a deterministic text generation approach and individual preferences are not supported. Since the formatters produce a consistent style,

each individual forecaster now has to sit down in front of hundreds of pre-generated forecasters which may or may not sit comfortably with their natural language style. While it has been made clear that the forecasters are not responsible for making stylistic changes to the GFE forecasts, nonetheless the forecasters are accustomed to taking full responsibility for the forecasts issued on their watch and as such often have strong opinions regarding the clarity and style of the language used (numerical forecast accuracy aside).

To make this really clear, it appears as though most meteorologically aware individuals have similar, but non-identical, mental analogies by which they think (and naturally, talk) about the weather. The public does not always share those analogies, which can result in confusion and disagreement. A similar issue might arise between a sound engineer and concert pianist – while both are concerned with music, they will often use entirely different terms and concepts to think and talk about it.

It is worth going through some examples in order to really see exactly what kind of problems are presented, and how significant they can be. We will first look at an example of this problem from the perspective of the forecasters being confronted with some actual examples of formatter output. Consider the following description of the wind:

“Winds northeasterly 15 knots tending northwest to southwesterly around midday”

This example complies fully with the requirements that resulted from a long period of discussion and evaluation of formatter performance prior to the GFE go-live date, yet it has emerged as a significant issue since that time. To naïve eyes, there may be little to distinguish this sentence from the preferred alternative:

“Winds northeast to northwesterly 15 knots tending southwesterly during the afternoon”

The difference lies in what the forecasters feel is not being communicated in the first example, namely that there is a frontal passage moving through which results in a generally southwesterly wind flow. Neither sentence is inconsistent with the data but one assembly of the sentence fits with the forecasters’ mental models of the evolving weather situation.

There are many more such examples. In some cases, it is clear that the forecasters' instincts are correct. In a few cases, the forecasters have become accustomed to using expressions which are outright unclear. It is in the middle that most of the debate occurs. There is also a tension between using simple, easy-to-understand forecasts and elegant expression. This is also where a lack of capability in the generation system limits what can be produced, and why fundamental linguistics research is still necessary. For example, the use of overly simple language can result in highly repetitive forecasts which are actually more difficult to read and comprehend.

The work by Reiter et al (2005) goes to some lengths to determine how effective automatically generated text is, compared against human-authored text and against human post-edited, automatically pre-generated text. Their findings are fairly clear – that human post-edited forecast text is preferred by readers. Their analysis of the reasons for this is in line with the opinions of the GFE formatter development team.

The major advantage of automatically generated text is a consistency which is not possible given the individual preferences of human forecasters. However, the human capacity for expression is significantly greater than that of automated systems. Presenting a first-draft forecast which uses consistent semantics generally means that a human forecaster will adopt the same semantics for the final forecast. They are able to improve upon the language of the automated system without compromising semantic consistency.

Reiter et al (2005) also delve into which particular aspects of forecast language are handled better by the automated system as opposed to human authoring. They find that in human-authored forecasts, some kind of term (for example verb choice), are based almost entirely on the data at hand, while others (such as times of day) are described poorly and inconsistently.

Conclusions

The text formatters provide a step forward in the number of forecasts which can be produced. By producing forecast grids, the forecasters enable the automated system to produce numerically-consistent forecasts for a larger number of locations than current forecaster resources permit.

A greater degree of consistency of the terms used to describe the weather is also achieved, with all terms used now having a consistent and clear link to underlying atmospheric conditions.

The greatest challenges to the formatters lie in their ability to extract the salient information from the statistics, then render that information into clear and elegant language, taking into account the desired length and level of detail for each forecast.

References

- De Smedt, K, Horacek, H. and Zock, M. 1996, *Architectures for Natural Language Generation: Problems and Perspectives*, in *Trends in Natural Language Generation: An Artificial Intelligence Perspective*. Berlin, Germany, Springer-Verlag pp. 17-46.
- Goldberg E, Driedger N and Kittredge R I 1994, *Using Natural-Language Processing to Produce Weather Forecasts*, IEEE Intelligent Systems, Vol. 9, No. 2, pp. 45-53.
- LeFebvre T, Mathewson M and Hansen T 2003, *The Rapid Prototype Project*, 19th International Conference on Interactive Information Processing Systems.
- Reiter E, Sripada S, Hunter J, Yu J and Davy I 2005, *Choosing Words in Computer-Generated Weather Forecasts*, Artificial Intelligence, Vol. 167, Issues 1-2 pp. 137-169.
- Stern H 2007, *Increasing Forecast Accuracy by Mechanically Combining Human and Automated Predictions using a Knowledge Based System*, 23rd Conference on Interactive Information and Processing Systems.
- Toth Z, Talagrand O, Zhu Y 2006, *The attributes of forecast systems: a general framework for the evaluation and calibration of weather forecasts, from Predictability of Weather and Climate* by Tim Palmer and Renate Hagedorn, Cambridge University Press.

POAMA SST Predictions for the Great Barrier Reef: Summer 2008/2009

Claire M. Spillman^A, Oscar Alves^B, Debra A. Hudson^C and Andrew N. Charles^D

^{ABCD}Centre for Australian Weather and Climate Research,

Bureau of Meteorology, Melbourne VIC 3001

c.spillman@bom.gov.au

Introduction

Coral bleaching has been observed sporadically in the Great Barrier Reef, Australia, since 1982. Anomalously high sea surface temperatures (SST) are recognised as the primary cause of mass coral bleaching events (Hoegh-Guldberg 1999; Lesser 2004). Advance warning of potential bleaching events allows for the implementation of management plans to reduce reef damage and maximise the potential for recovery (Marshall and Schuttenberg 2006). Predictions on a seasonal time-scale are the most practical for reef managers, as strategies can be implemented at the start of summer prior the onset of bleaching. Seasonal dynamic forecasts of SST anomalies in the GBR region were generated in real time as an experimental product using the Predictive Ocean Atmosphere Model for Australia (POAMA) at the Australian Bureau of Meteorology for the summer of 2008-2009. These are updated daily on the website <http://poama.bom.gov.au>. POAMA is a seasonal coupled ocean-atmosphere and data assimilation ensemble forecast system, developed by the Bureau of Meteorology and CSIRO, and has been run operationally since 2002. For more details of the model setup and forecast generation see Spillman and Alves (2009).

In the model hindcast set of SST anomalies for the period 1980-2006, POAMA exhibits useful skill in the GBR region in January-March up to 2-3 months ahead, both spatially and in areal averages (Spillman and Alves, 2009). The ensemble generation technique differs slightly between the hindcast and real-time operation systems but skill is expected to be relatively similar. In the real-time system, a nine month

forecast is produced each day, with the POAMA monthly outlooks based on an ensemble of the forecasts from each of the 30 most recent days. The variability of the results among forecasts gives an indication of the uncertainty in the future evolution of the climate system. This provides information as to the probability distribution of future conditions and allows for more informed management decisions.

This paper gives an overview of SST in the GBR for the summer of 2008/2009 and the skill of POAMA in predicting these conditions in real-time. Accurate seasonal SST forecasts for this region will be an invaluable tool for the future management and conservation of the reef.

Observed summer conditions

Initial observations in the GBR region suggested the summer of 2008/2009 could be unusually warm. Observed satellite monthly SST anomalies from the Reynolds OI.v2 1° analysis showed warm anomalies as early as October with very warm conditions occurring in December, up to 1.3°C above the long term December monthly average temperatures (Figure 1). These values are similar to those that occurred in December 1997 and 2001, which marked the start of mass coral bleaching during those summers. However, temperature anomalies then cooled significantly during January and February 2009, with average SST conditions similar to long term climatological values by February (Figure 1). The primary driver of these cooler anomalies was the onset of the monsoon season in January 2009, which brought heavy rain, increased wind and enhanced levels of cloudiness. Storms in January

and February caused record levels of rain and extreme flooding over land to the west, with flood water plumes covering large areas of the GBR.

The timing of the onset of the Australian monsoon and development of its bursts and breaks is often influenced by the Madden Julian Oscillation (MJO) (Wheeler et al. 2009). The MJO is a global-scale feature of the tropical atmosphere with associated weekly to monthly periods of alternating active and inactive rainfall over parts of Australia and is generally best developed in summer. Active periods bring broad areas of persistent rain, while break periods are generally drier, and often hotter, with only isolated thunderstorms and rain systems.

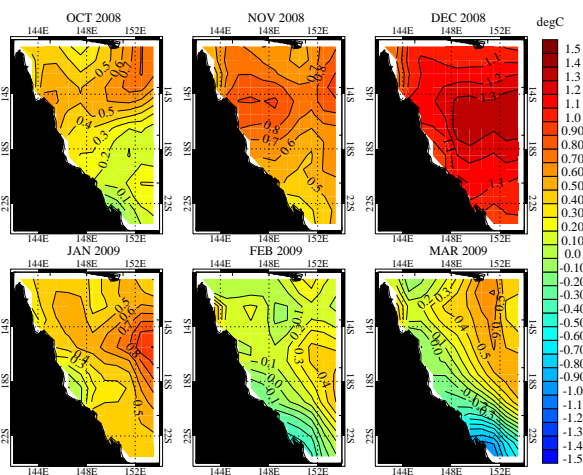


Figure 1. Monthly Reynolds OI.v2 1° SST anomalies in the GBR region for October 2008 - March 2009.

In summer 2008/9, according to the Bureau of Meteorology Weekly Tropical Climate Note (<http://www.bom.gov.au/climate/tropnote/tropnote.shtml>), tropical convective activity extended eastward to northern Australia during December, producing heavy widespread rainfall and thunderstorms. This activity persisted around the Maritime Continent region until the middle of January, seemingly in response to the broader atmospheric tropical circulation and La Niña-like conditions, with little apparent MJO modulation. Around the middle of January activity picked up in the central Indian Ocean while in near-equatorial regions of the Maritime Continent it became relatively suppressed, indicative of renewed modulation by the MJO. By the end of January, a tropical low had developed on the

monsoon trough and was positioned over the southern Gulf of Carpentaria. This low deepened slowly and produced further heavy rainfall in already flooded areas in the first half of February. From the middle of February this activity waned somewhat, and northern Australia returned to a relatively suppressed MJO phase for the remainder of the month. Rainfall in much of Australia's tropical region in early March was not enhanced during the active MJO phase.

POAMA Summer Outlook

Model outlooks issued 1st December 2008...

The outlook for the summer of 2008/2009 in the GBR region was initially quite warm, with the indications that conditions may be sufficient to induce coral bleaching. POAMA real-time forecasts for the coming summer months, available on 1st December 2008, suggested anomalous warmth over the GBR region with SST anomalies up to 0.8°C in December and January (Figure 2). Observed anomalies in December and January were also warm though December was considerably warmer than the model ensemble mean indicated. In January the model predicted similar anomalies as those observed, though the outlook was slightly warmer along the coast. However, for February the model forecast was considerably warmer than observed anomalies. This suggests that the model did not predict the timing and location of the monsoon onset which led to cooler temperatures in January and February.

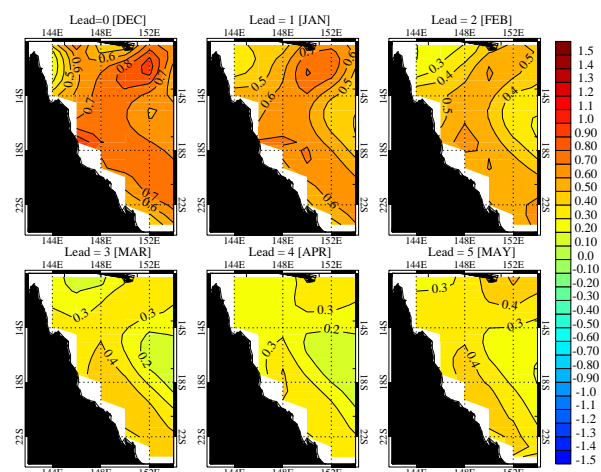


Figure 2. POAMA SST anomalies (ensemble mean) in the GBR region for December 2008 to February 2009 in the official outlook issued on 1st December 2008.

The GBR Index is the areal average of SST anomalies in the GBR region and has been shown to be a useful indicator of average conditions in the area (Spillman and Alves 2009). Use of such an index also allows us to show both the ensemble mean and the spread of the individual forecasts that made up the ensemble. The predicted GBR Index showed warmest conditions occurring for December with relative cooling over the region occurring in January and February (Fig 3), but with the interquartile range of values still falling within the model's upper tercile. Observed GBR Index values showed a similar trend with peak anomalies occurring in December, values which were captured within the model ensemble spread i.e. the range of the 30 forecasts used to make up the ensemble. Although the spatial patterns of observed and forecast SST anomalies were quite different, observed GBR Index values for January and February were quite close to the ensemble mean.

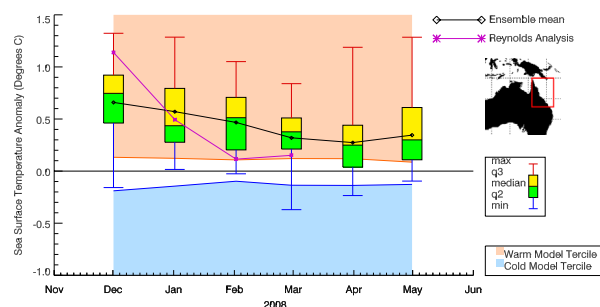


Figure 3. POAMA monthly GBR Index values for December 2008 to May 2009 in the official outlook issued on 1st December 2008, with the distribution by quartiles of the ensemble composed of the last 30 forecasts. Overlaid is the ensemble mean (black) and the observed Reynolds GBR index (pink). The shading indicates upper and lower climatological terciles from the POAMA v1.5 hindcasts.

Model outlook issued 1st January 2009 ...

POAMA real-time forecasts issued on 1st January 2009 for January-March 2009 also indicated anomalously warm conditions over the GBR region, with SST anomalies up to 1.2°C in January (Figure 4). These values were comparable to the monthly SST anomalies during the GBR bleaching events of 1998 and 2002, causing some concern amongst reef managers that a similar event could have occurred. However, observed monthly SST anomalies in January were considerably cooler than those

forecast by the ensemble mean from POAMA. This was due to the onset of the monsoon in mid-January which brought anomalously high rainfall, increased winds and elevated cloudiness, and subsequently cooler sea surface temperature anomalies. Most of the POAMA ensemble members were not able to capture the timing of the monsoon onset, hence a warmer ensemble mean, but the model forecast for February and March still indicated cooling, as was observed, though the amount of cooling was underestimated.

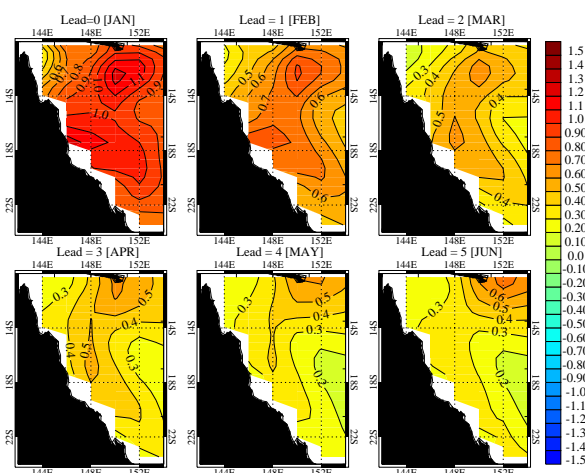


Figure 4. POAMA SST anomalies (ensemble mean) in the GBR region for January- March 2009 in the official outlook issued on 1st January 2009.

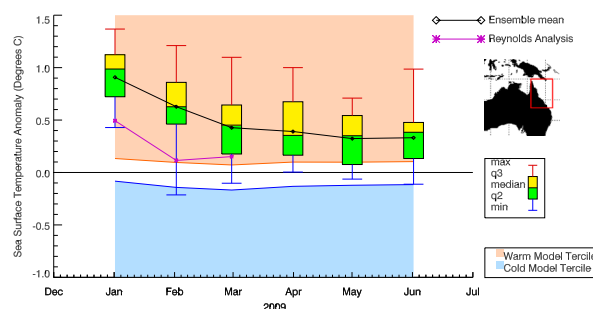


Figure 5. POAMA GBR Index values for January-June 2009 in the official outlook issued on 1st January 2009, as per Figure 3.

The predicted GBR Index available on 1st January (Figure 5) again indicated higher than observed average SST anomalies in the region for January, with the observed value captured within the model ensemble spread. This indicates that a few of the ensemble members did cool rapidly as observed, but the majority cooled more slowly.

All the ensemble forecasts for January were in the upper model tercile, corresponding with the observed value falling in the upper observed tercile.

Model outlook issued 1st February 2009...

The official model outlook available on 1st February 2009 predicted cooler temperatures for February-April (Figure 6) than outlooks from 1st December and 1st January. This may be explained by the fact that the model initial conditions included information of the observed monsoon conditions and cooler SSTs that occurred in January. However, observed February conditions were significantly cooler than ensemble mean forecasts indicated and close to climatological values (Figures 1 and 6). The monsoon trough was located over the northern Cape York Peninsula for most of the month, generating showers and thunderstorms, and also rain areas over most of the central and northern tropics (Bureau of Meteorology Seasonal Climate Summary for Queensland: Summer 2008-2009 <http://www.bom.gov.au/climate/current/season/ql/archive/200902.summary.shtml>). Extreme flooding and Cyclone Ellie in early February contributed to cooler sea temperatures, features which are not captured by the model.

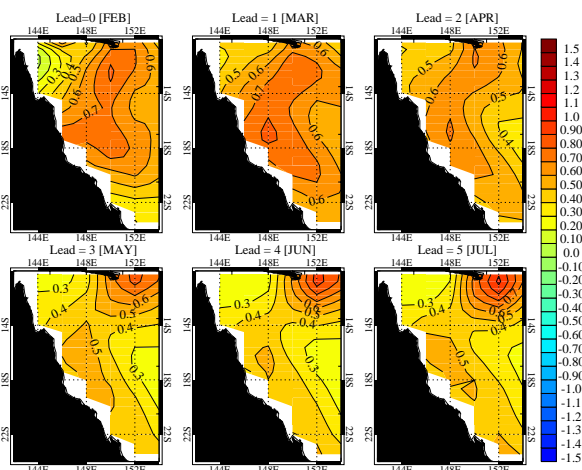


Figure 6. POAMA SST anomalies (ensemble mean) in the GBR region for February-April 2009 in the official outlook issued on 1st February 2009.

The corresponding ensemble mean forecast for the GBR Index issued in February (Figure 7) indicated average anomalies around 0.5 °C for the following few months, though with relatively large degree of spread within the ensemble

members, particularly for March. The observed values for February and March were within the ensemble spread though at the lower limit. Both observed and model values fell within their respective upper terciles.

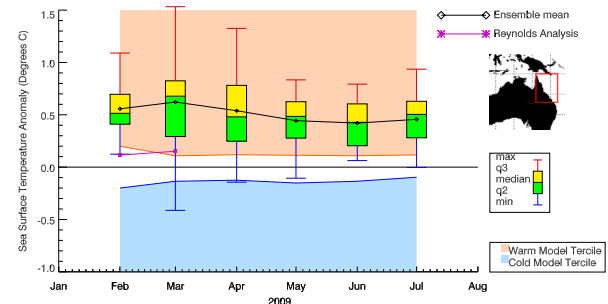


Figure 7. POAMA GBR Index values for February-July 2009 in the official outlook issued on 1st February 2009, as per Figure 3.

Summary

Forecasts from POAMA correctly predicted warmer than usual conditions in the GBR region for the summer of 2008/2009. Both observed and ensemble mean forecasts consistently fell within their respective upper terciles. Observed values were captured within the ensemble spread for all months, with some approaching the ensemble mean. However, while a few of the ensemble members did indicate the rapid cooling following the monsoon onset, most ensemble members did not, indicating that the observed outcome was possible but not the most likely.

The large spread in the model ensemble is most likely due to different ensemble members producing different realisations of intraseasonal variability. For example, the MJO has a relatively short time scale of 30-60 days, the current belief is that it cannot be predicted beyond 1-2 weeks in the future. The model ensemble members can therefore be interpreted as sampling different possible future realisations of this higher frequency variability, and large spread indicates a limit on our ability to predict the future.

References

Hoegh-Guldberg, O., 1999. Coral bleaching, climate change and the future of the world's coral reefs. Review. Marine and Freshwater Research, 50:839–866.

Lesser, M.P., 2004. Experimental biology of coral reef ecosystems. *Journal of Experimental Marine Biology and Ecology*, 200:217–252.

Marshall, P.A., Schuttenberg, H.Z., 2006. A Reef Manager's Guide to Coral Bleaching. Great Barrier Reef Marine Park Authority, Australia pp167 (ISBN 1-876945-40-0).

Spillman, C.M., Alves, O., 2009. Dynamical seasonal prediction of summer sea surface temperatures in the Great Barrier Reef. *Coral Reefs*, 28:197-206.

Wheeler, M.C., Hendon, H.H., Cleland, S., Meinke, H., Donald, A., 2009. Impacts of the Madden-Julian oscillation on Australian rainfall and circulation. *Journal of Climate*, 22:1482-1498.

Weather-Band Coastal Sea Level Anomalies along Australia's Southern Shelves: Bluelink OceanMAPS

Andy Taylor

Centre for Australian Weather and Climate Research

Bureau of Meteorology

a.taylor@bom.gov.au

Introduction

This letter considers the representation of weather-band coastal sea level anomalies (SLA) and coastally trapped waves (CTWs) along Australia's southern shelves using the current implementation of the Bluelink OceanMAPS prediction system (Brassington et al. 2007). The aim is to extract specific features of coastally propagating SLA from the OceanMAPS behind-real-time analysis data, and to perform some comparisons with the established literature. This study does not explore the many possible paths of enquiry in any depth and in fact is deliberately confined in scope in line with the Research Letter format.

Background

Australia's southern shelf region between Cape Leeuwin and Bass Strait represents possibly the world's longest zonal mid-latitude ocean shelf (Ridgway & Condie 2004; Middleton & Bye 2007). Coastal waters in the region are typically mesotidal and subject to relatively powerful weather-band sea level fluctuations. The spectral weather-band is defined here as ranging from about 2-30 days, which excludes the important seasonal cycles described by Ridgway & Condie (2004) and others. Figure 1 shows the observed coastal sea level spectrum overlaid with the official tide prediction spectrum for the National Tidal Centre tide gauge located at Thevenard SA. Weather-band coastal sea level phenomena contribute to 'storm tide' conditions that can impact coastal communities and operations. For instance, negative SLA events can limit under-keel clearance for ship operations at South Australian Ports whilst positive SLA contributes to events such as the seaweed intrusion of urban drains at Port Lincoln (Adelaide Advertiser, 2009). This topic is operationally relevant as the

South Australian office of the Bureau of Meteorology issues storm tide advice products and as these phenomena fall within the forecast time scales of OceanMAPS. Note however, that this letter considers only behind-real-time OceanMAPS analysis data and *not* forecast data.

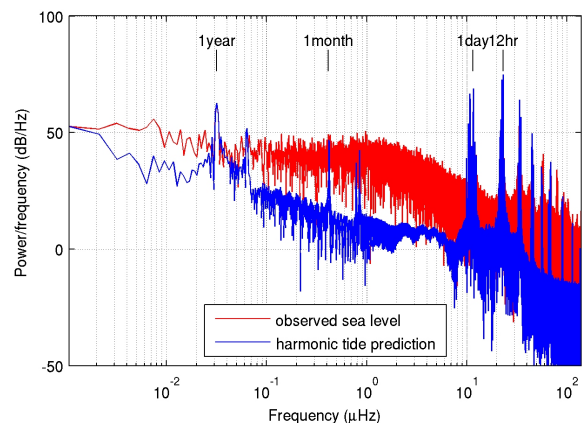


Figure 1. Sea Level Spectra from tide gauge at Thevenard SA.

Coastally Trapped Waves in the Region

CTWs represent a hybrid class of sub-inertial frequency long waves combining Kelvin and shelf-wave mechanisms. Overviews of the theory are given in Gill (1982) and Mysak (1980). The present study considers only 1st mode barotropic theory and makes broad comparisons to the manifest total SLA data. Thus the effects of stratification and other details, though actually modelled within OceanMAPS are not treated directly. Similarly, no attempt has been made to decompose the total SLA signal into modal contributions. One reason for choosing this region was prediction skill in OceanMAPS identified by Nader et al. (2009) who compared SLA to observations of sea-level from tide gauge stations.

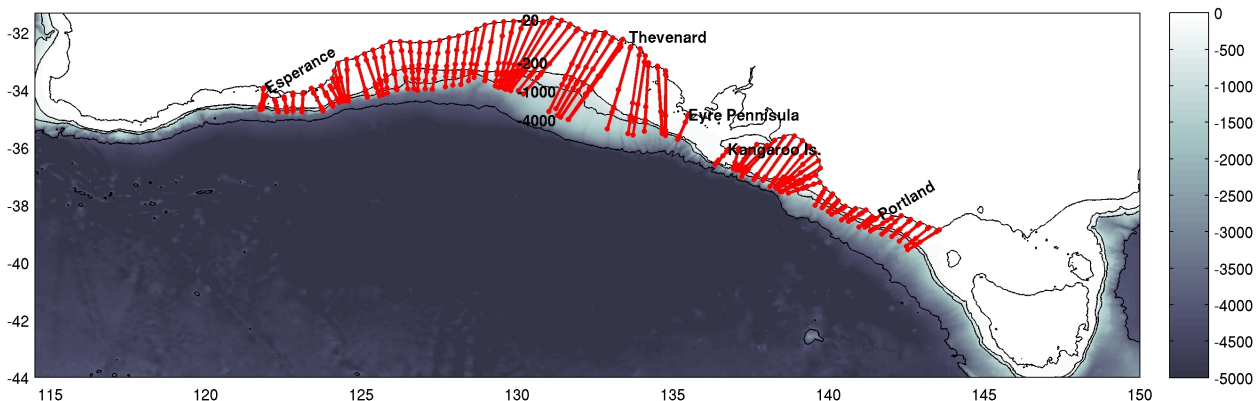


Figure 2. Bathymetry along the Southern Shelves. The 4000 m, 1000 m, 200 m & 20 m contours are shown. Red lines are cross-shore directional transects derived via the stepping algorithm.

The second reason was that Middleton & Bye (2007) and Church & Freeland (1987) [hereafter C&F] specifically discuss CTWs in the region. Both of these papers raise the question of suspected resonance between eastward propagating CTWs and similarly propagating forcing wind systems. In addition, Ridgway & Condie (2004) specifically addressed the relative importance of wind stress forcing of SLA, though on seasonal time scales. The present letter deliberately presents results in a manner that mirrors several of the figures in C&F.

Data under consideration

The results presented are based on just over 500 days of OceanMAPS behind-real-time analysis. OceanMAPS does not include variation in sea level driven by changes in atmospheric sea level pressure or that generated by the astronomical tides. OceanMAPS mainly represents sea level driven by surface winds and mesoscale baroclinic forces. Wind stresses used to drive the model are 3 hourly surface winds the GASP NWP system (Seaman et al. 1995).

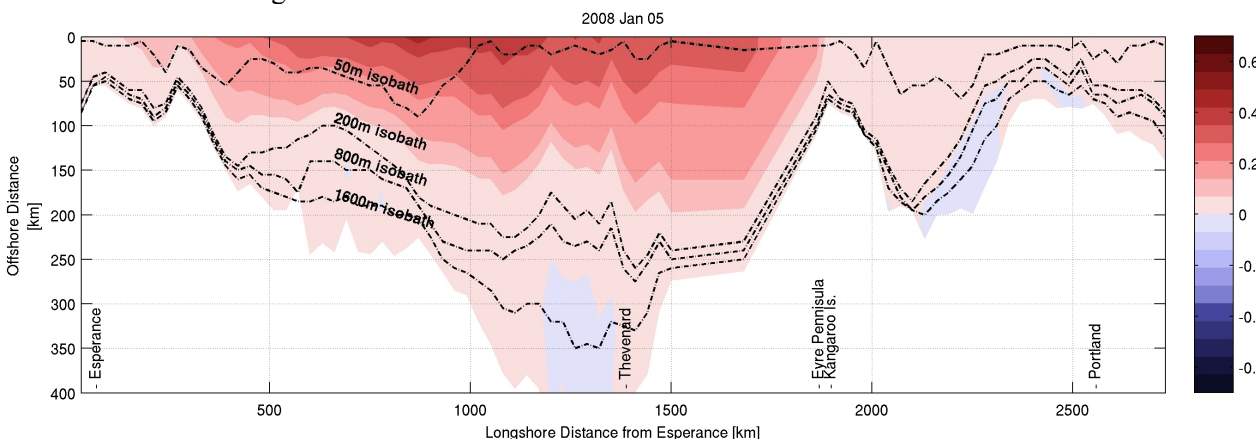


Figure 3. Snapshot of a CTW in new coordinates. Colour scale indicates weather-band SLA in metres.

Pre-processing of data

The series of data pre-processing steps undertaken are summarized as follows: Firstly, the wind stress data were reduced to daily means corresponding to the daily mean SLA

data and the respective overall sample means were subtracted from each grid point. Then, the data were transformed to the new long/cross-shore coordinates X/Y. By averaging the X component of wind stress data between the coast and the 200 m isobath a

representative long-shore coastal wind stress field was derived. Finally, a high pass filter was applied to remove signal power for periods longer than around 30 days.

Development of coordinate system

The common framework adopted in the literature is that of a long/cross-shore coordinate system. Such coordinates are inherently problematic when applied to realistic geography (Allen 1980, 436; Mandelbrot 1967). For the present work, a topographic based stepping algorithm was developed. In short, the coastline was stepped along at known separations to develop the long-shore path length. From each point along this path the bearing towards the closest shelf break was found, and the offshore depth profile along this bearing then used to define the cross-shore coordinates. Figure 2 shows the original bathymetry and the resultant series of great circle paths in the cross-shore direction. Note that a discontinuity in the long-shore step length was introduced in order to jump over the SA Gulf region for simplicity. Figure 3 shows a snapshot of a positive amplitude CTW in the new coordinates. The y-axis has been oriented with the coastal boundary at the top. In this image the spatial extent of the event complies with expectations of having a cross-shore length scale of $O(100\text{ km})$ and being elongated in the long-shore direction.

Weather band power: long-shore variation

Following C&F (Figure 2) the long-shore variation of weather-band SLA at the coast, hereafter denoted as η_{WB} , is presented in Figure 4. The corresponding plot for long-shore wind stress (τ_{WB}) is shown in Figure 5. The plots indicate variance per period band at each location. The relative amplitudes at Esperance, Thevenard and the entrance to Bass Strait, as well as the peak power of 7-8 days are broadly consistent with C&F. Inspection of Figures 3, 4 & 5 shows significant spectral overlap between τ_{WB} and η_{WB} , stronger variations of τ_{WB} in the west and a positive correlation between shelf width and η_{WB} variance.

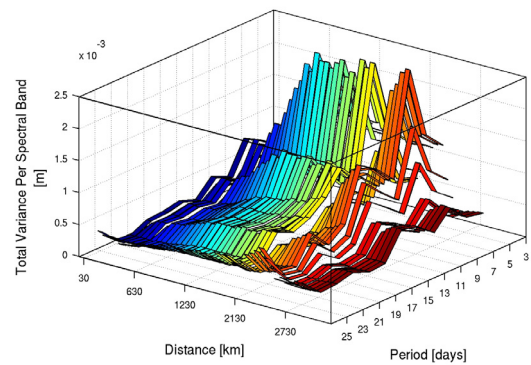


Figure 4. Long-shore evolution of η_{WB} spectra: variance per period band.

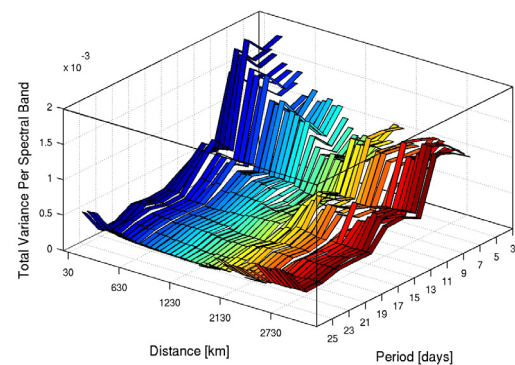


Figure 5. Long-shore evolution of τ_{WB} spectra.

Propagation speed

In the present context, two very simple estimates of long-shore wave propagation speed are used as a reference. Firstly, the barotropic Kelvin wave mechanism as estimated by the equation for shallow water wave phase speed $c = \sqrt{gH}$. This gives a range of 10-45 m/s between the 10 m and 200 m isobaths. The second is that for the shelf wave mechanism $c = fL$, where f is the Coriolis parameter and L is the shelf width. Giving a range of about 5-20 m/s. Barotropic CTWs are considered to be a hybrid of these mechanisms.

Following C&F (Figure 4) Figure 6 indicates the negative lag in days between η_{WB} at Portland in the East and each point along the long-shore path.

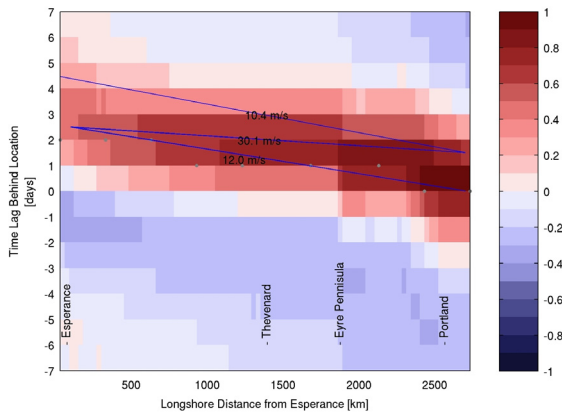


Figure 6. Lagged correlation diagram comparing η_{WB} (m) to the reference of Portland in the East.

The diagonal concentration of maximal correlation is consistent with expectations of unidirectional generally eastward propagation. The temporal resolution of 1 day imposes an upper limit of around 30 m/s on interpretations of wave speed from this type of diagram. This limits the ability to distinguish between fast CTWs and broad storm surges. That said, the series of hand drawn estimates indicate a range of around 10-30 m/s, which is considered consistent with simple analytical estimates and discussion above.

Wind Stress Forcing and Resonance

Following Gill (1982, pp 399; 1973), only the long-shore component of the wind stress close to shore is of primary importance. Figure 7 shows matching Hovmöller diagrams for η_{WB} and τ_{WB} . Figure 8 is a close-up of the same diagram. Assessed visually, the figures indicate generally matching patterns of eastward propagation. The amplitude of τ_{WB} appears to be relatively higher in the west, whilst η_{WB} appears to generally peak at points of widest shelf width. Possible propagation speeds are indicated by hand-drawn lines, which given the limitations discussed above again show a 10-30 m/s range.

Figure 9 shows lagged cross-correlations between τ_{WB} and η_{WB} time series at each point along the coast. The pattern of high correlations is concentrated and asymmetrical with respect to lag, with a weak tendency to slightly longer lags in the east.

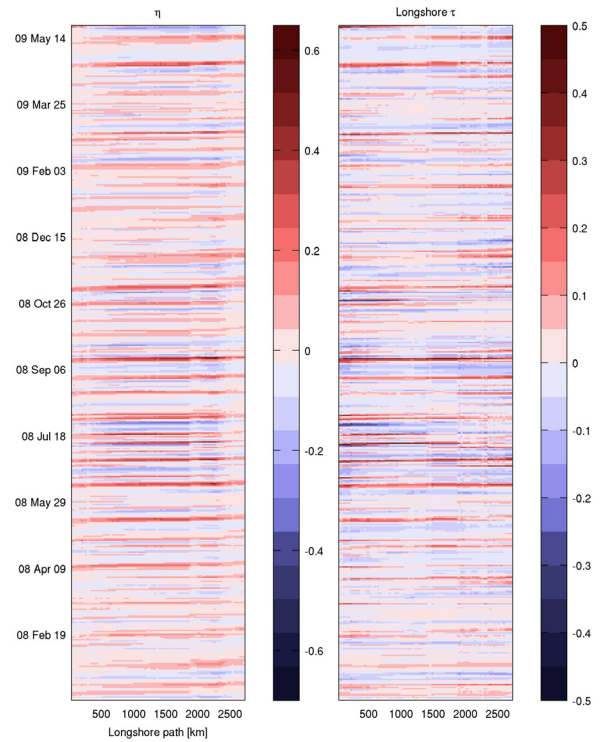


Figure 7. Hovmöller plots for η_{WB} [m] and τ_{WB} (N/m^2)

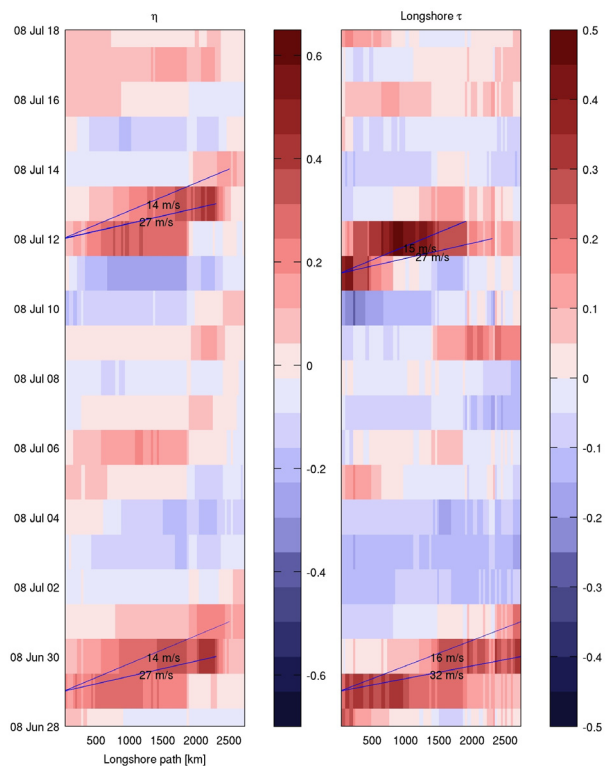


Figure 8. Close-up Hovmöller plots: η_{WB} & τ_{WB} .

Despite limitations of time resolution and dataset length, Figures 8-9 are considered consistent with a scenario in which near resonant forcing of η_{WB} by τ_{WB} does often occur, with η_{WB} patterns typically propagating a little slower than τ_{WB} (+ve lag trend) but on occasion a little faster (-ve lags).

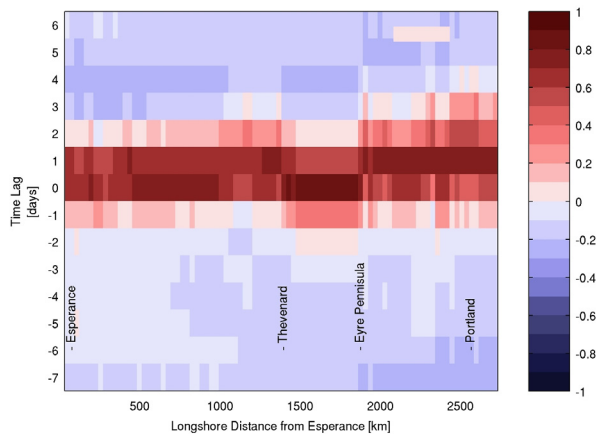


Figure 9. Cross correlation diagram: η_{WB} vs. τ_{WB} .

Conclusions

Other work has established the skill of OceanMAPS in representing weather-band coastal SLA on Australia's Southern shelves (Nader et al. 2009). The present letter shows that these coastal SLA variations in the OceanMAPS data can be identified as CTWs. The propagation, phase speed, length scales and forcing of these CTWs are broadly consistent with the literature. The fact that only daily mean values for SLA are presently made available from OceanMAPS has limited the present study somewhat. This limitation may also impact future work towards 'total sea level' predictions and improved storm tide warnings. It is thus recommended that higher frequency output be implemented for a selection of coastal locations.

References

- Adelaide Advertiser May 24 2009. "Repairs needed after Port Lincoln flood"
- Brassington, G. B., T. Pugh, C. Spillman, E. Schulz, H. Beggs, A. Schiller and P. R. Oke, 2007. "BLUElink> Development of operational oceanography and servicing

in Australia." *Journal of Research and Practice in Information Technology*. **39**:151-164

Brink, K.H. 1982. "A Comparison of Long Coastal Trapped Wave Theory with Observations off Peru." *Journal of Physical Oceanography* **12**:897-913

Church, J.A. and Freeland H.J. 1987. "The Energy Source for the Coastal-trapped waves in the Australian Coastal Experiment Region." *Journal of Physical Oceanography* **17**:289-300

Chapman, D.C., 1983. "On the Influence of Stratification and Continental Shelf and Slope Topography on the Dispersion of Subinertial Coastally Trapped Waves." *Journal of Physical Oceanography* **13**:1641-1652

Clarke, A.J., 1977. "Observational and Numerical Evidence for Wind-Forced Coastal Tapped Long Waves." *Journal of Physical Oceanography* **7**:231-247

Ridgway K.R. and Condie S.A. 2004. "The 5500-km-long boundary flow off western and southern Australia." *Journal of Geophysical Research* **109**:CO4017

Gill, A.E., Schumann E.H., 1974. "The Generation of Long Shelf Waves by the Wind" *Journal of Physical Oceanography* **4**:83-90

Gill, A.E., 1982. *Atmosphere-Ocean Dynamics*. Academic Press London.

Huthnance, J.M., 1987. "Effects of Longshore Shelf Variations on Barotropic Continental Shelf Waves, Slope Currents and Ocean Modes" *Progress in Oceanography* **19**:117-220

Mandelbrot, B.B., 1967. "How long is the coast of Britain? Statistical self-similarity and fractional dimension." *Science* **156**: 636-638

Middleton, J.F. and Bye, A.T., 2007. "A review of the shelf-slope circulation along Australia's southern shelves: Cape Leeuwin to Portland." *Progress in Oceanography* **75**:1-41

Mysak, L.A., 1980 "Topographically Trapped Waves." *Annual Review of Fluid Mechanics* **12**:45-76

Nader, J.R., Taylor, A.J., Brassington G.B. (Expected publication 2009) "Operational Non-Tidal Sea Level

Forecasts: Preliminary skill assessment of Bluelink OceanMAPS against SEAFRAME coastal tide gauges." *CAWCR Technical Report*

Seaman, R., W. Bourke, P. Steinle, T. Hart, G. Embery, M. Naughton, L. Rikus. 1995. "Evolution of the Bureau of Meteorology's Global Assimilation and Prediction System Part 1:Analyses and Initialization." *Aust. Met. Mag.* **44**:1-1.

Numbers and Genesis Locations of Tropical Cyclones in the NOAA IBTrACS Archive

Ian G. Watterson

CSIRO Marine and Atmospheric Research,

Aspendale, Australia

ian.watterson@csiro.au

Introduction

In support of a new study of the variability in tropical cyclone (TC) numbers, as diagnosed from a long simulation of the CSIRO Mk2 climate model (Hunt and Watterson 2009), the new NOAA IBTrACS archive of all recorded TC tracks worldwide was recently analysed. With the observational component in that study being limited to a climatological distribution of cyclone genesis, the present brief paper provides further results, in addition to promoting the archive to readers.

Hunt and Watterson (2009) followed two earlier studies by using the Seasonal Genesis Parameter (SGP) of Gray (1975) as a surrogate for TCs. While this relates to a broadly realistic distribution, the SGP appears to diagnose a relatively large proportion of events for the southern hemisphere (SH). Ryan et al. (1992) suggested that this may be partly due to some cyclones being not detected in the SH in early years of the record, and it is worthwhile examining this further with the latest observational data. With the apparent increase in numbers of intense TCs over the period 1975 to 2004 (e.g., Webster et al. 2005), the presence of trends in the archive is of particular interest.

The following sections briefly describe the archive and the method used here. Time series of event numbers in different basins as a function of wind intensity are then considered. Finally, climatological maps are presented. Given the recent comprehensive review of TCs by Knutson et al. (2009), references are made only to earlier studies of particular relevance. Some limited comparisons are made with previous data sets.

Data

The IBTrACS archive is described by Knapp et al. (2009), Kruk et al. (2008) and the website www.ncdc.noaa.gov/oa/ibtracs. The name stands for *International Best Track Archive for Climate Stewardship*. The aim is to provide a single global data set for tropical cyclone research. Data from some eleven TC agencies around the globe were collected and objectively combined. The total number of storms currently archived is 8163, the earliest being from 1848.

The data set includes the position of the storm centre, maximum sustained wind (MSW) averaged over 10 minutes (the international standard) in knots, and central pressure, all every six hours. The coverage of storms is, naturally, incomplete in the early years, and parameters are often unavailable, except in more recent years. Kruk et al. (2008) provide some details of the methods used to address data limitations, as well as basic statistics on the tracks.

The data set is freely available from the website in various formats. Version 1, obtained as the file [Allstorms.ibtracs.v01cor-r01.nc.gz](http://www.ncdc.noaa.gov/oa/ibtracs/v01cor-r01.nc.gz) on 20-2-2009, is analysed.

Method

Following the approach of Watterson et al. (1995), in their study of the SGP, the position of cyclone origin is taken to be 'the first recorded location of a developing depression that later became a tropical cyclone with MSW' reaching a certain criterion. They cited the wind speed as 'at least 20-25 m s⁻¹, or 38.9 to 48.6 knots, presumably for the U. S. period of 1 minute. Reducing the first value by the factor 0.88 (Kruk et al. 2008) to relate to the longer period, gives

34 knots. The IBTrACS website gives statistics for both 30 knots ('tropical storm strength') and 54 knots (U. S. category 1 strength). The 30 knot speed is used as the standard here. Storms with MSW not reaching 30 knots are present in the data, as well as many earlier storms for which there are no wind data. In some cases there is only one storm position available. The various measures of TC intensity are related to Australian TC categories on the Bureau of Meteorology website (www.bom.gov.au/weather/cyclone/faq).

I have written a Fortran program that reads the data for each storm and determines this genesis location, for storms with MSW reaching various criteria. The code accumulates locations within the standard 5 degree latitude-longitude squares (centred on 2.5°N, 0.0°E, and so on). This is done for each of four seasons, starting with January-March (JFM), with the one month shift allowing for a lag in the oceanic temperature. It is then simple to sum numbers of genesis events across different regions or 'ocean' basins, specified here using latitude and longitude bounds and not excluding land, as detailed in the Appendix. Note that each hemisphere includes squares not in any of the seven basins. The sums are simply described as numbers of TCs, although later behaviour along the track is disregarded.

With genesis occurring largely in the warmer months, IBTrACS uses the term 'season' to mean the year centred on these months. For the Northern Hemisphere (NH) this is simply the calendar year. For the SH the months July-December are considered part of the season that is known by the number of the following year. For instance, the annual number in the SH depicted here for year 1990 includes the events from JFM and April-June (AMJ) of 1990, as well as the (likely few) events from July-September (JAS) and October-December (OND) of 1989. For simplicity, global annual numbers are calculated as the sum of the SH and NH numbers.

Note that the calendar year, and nearest day, latitude and longitude of the first position are coded in the storm serial number from the data set.

Numbers of TCs in the Archive

The first storm that is provided with a MSW that exceeds 30 knots is in the NH season of 1851.

Graphs of the time series shown here start at 1850. There are four other storms included before 1851 (all in the SIO basin), and 16 in the incomplete season 2008, which is excluded. For this criterion 5482 storms are counted over 1851-2007. Time series of annual global numbers for this MSW, and others, are shown in Figure 1a. Clearly, there are relatively few events selected in the early years, even through the WW2 period.

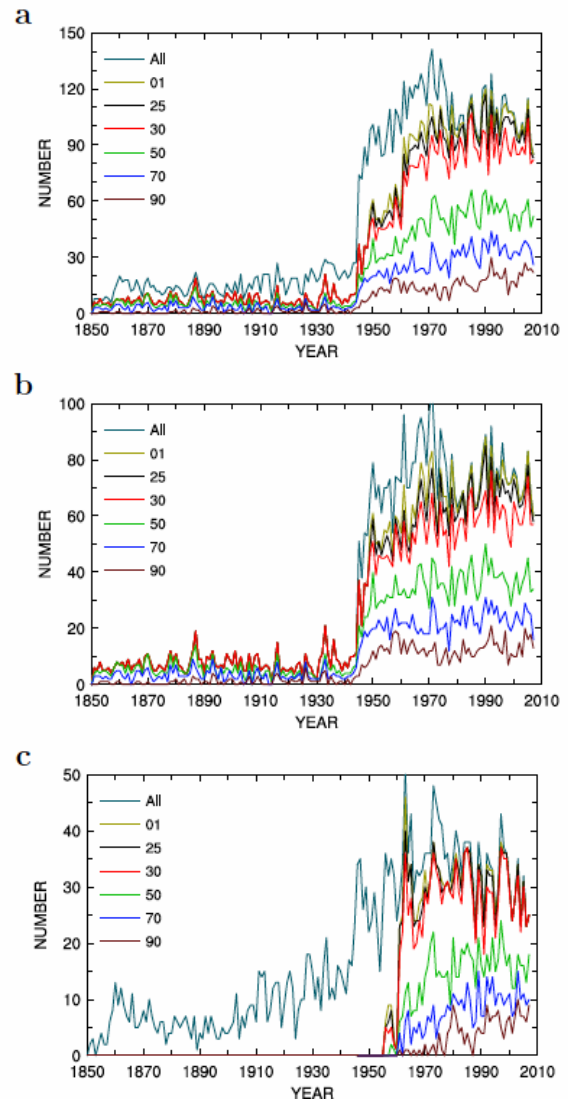


Figure 1. Numbers of cyclones for each year (a) over the globe, and within the (b) NH and (c) SH, for a range of speed criteria. The label 'All' denotes all storms, even those with missing MSW, and '01' allows any MSW above zero. Note that lines for lower speeds are obscured, when the numbers are the same.

From an earlier NOAA TC data set, Watterson et

al. (1995) found the average number during the period 1967-1986 to be 95 per year, which was slightly down on the average for 1952-1971 from Gray (1975), with both included in Table 1. The IBTrACS average for these periods are 87 (Table 1) and 66. Among other detection issues discussed by Kruk et al. (2008), uncertainties in wind speeds contribute to such differences. Hunt and Watterson (2009) relaxed the criterion to 25 knots. This allows 489 more storms in total, and boosts the 1967-1986 average to 96, making it more compatible with the earlier result and also the SGP statistics, including those reproduced in Table 1 from Watterson et al. (1995). In fact, in the global numbers of Figure 1a, the annual values are raised only in years after 1948.

Table 1. Numbers of genesis events per year (to the nearest integer), over the globe and within each hemisphere. Also given is the hemispheric Ratio, NH divided by SH. Various observational data sets and years are used. IB is the present IBTrACS data, with the wind criteria noted. Numbers inferred using the SGP are then given. Gray refers to Gray (1975). WER is from Watterson et al. (1995), using atmospheric data simulated by a model with sea surface temperatures prescribed. They also estimated the Gray, SGP numbers.

Data	Globe	NH	SH	Ratio
Gray, 1952-1971	99	67	32	2.09
NOAA, 1967-1986	95	64	31	2.03
IB (All), 1952-1971	111	78	32	2.44
IB (30), 1967-1986	87	57	30	1.93
IB (25), 1967-2007	97	67	30	2.21
IB (30), 1967-2007	88	59	29	2.07
IB (50), 1967-2007	53	37	16	2.33
IB (30), 1998-2007	88	59	28	2.10
Gray, SGP	109	62	47	1.32
WER 1979-1988	141	84	57	1.47

Allowing any MSW to pass (a nominal 0.0001 knots was used) adds a further 268 storms, also after 1948. On top of these, there are a further 1908 storms in the data set for 1848-2007 with no winds supplied. The annual numbers for all storms are also graphed, and it is evident that the no-wind storms boost numbers even into the 1970's. The all-storm average for 1952-1971 (Table 1) closely matches the Gray SGP global result.

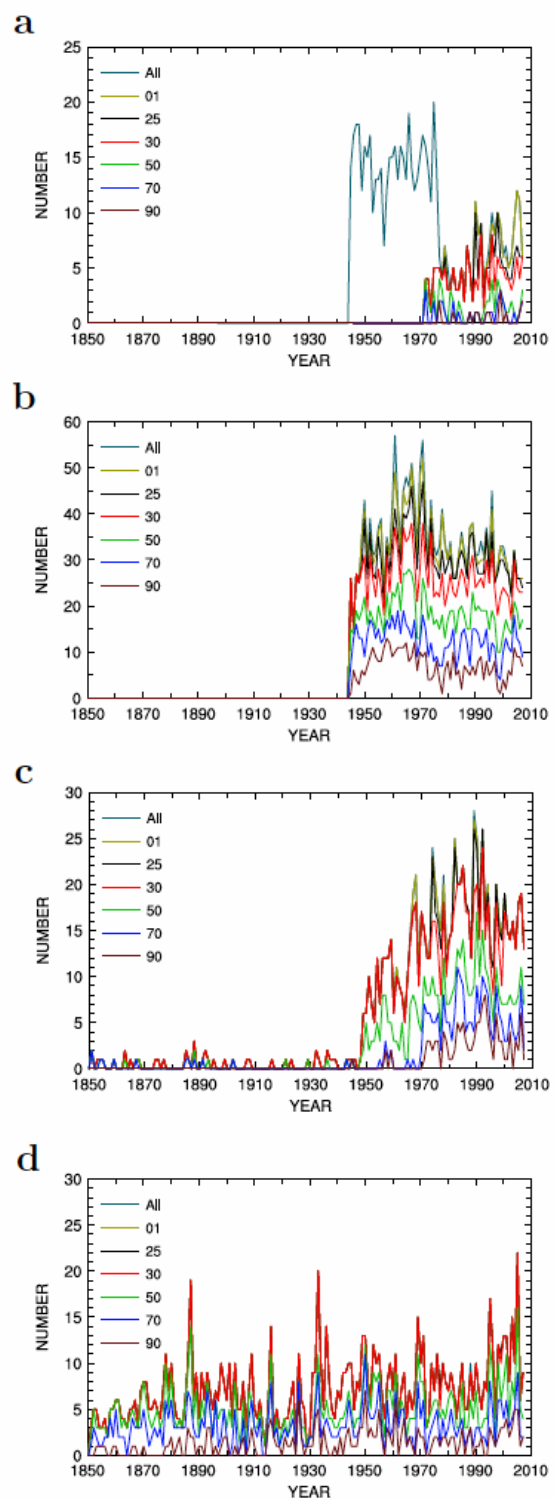


Figure 2. Numbers of cyclones for each year within NH regions (a) NIO, (b) WNP, (c) ENP, and (d) NA, for a range of speed criteria.

The numbers within each hemisphere are shown in Figure 1b (NH) and 1c (SH) as well as Table 1. It can be seen that there is no boost in numbers from lowering the criteria below 30 knots after 1944 in the NH. In the SH, there are no MSW data prior to 1956. In both hemispheres, numbers of archived storms increase rapidly after 1944.

Clearly these large temporal variations relate to the availability of the data (Kruk et al. 2008). The character differs between the basins, also, as can be seen in Figs. 2 and 3. In the North Indian Ocean basin (NIO, Figure 2a) there are many events with no MSW included during the 1940s to 70s, but few later. Events with MSW start in 1972. Most events in the Pacific (Figure 2b, c), are provided with a MSW that exceeds 25 knots. However, the numbers prior to 1973 in the WNP may be artificially increased by overestimated wind speeds (Emanuel 2005, supplementary material). For the North Atlantic region (NA, Figure 2d), over the ocean there are no storms in the archive with MSW not reaching 30 knots. While the detection methods changed in time (e.g., Landsea 2007) there are events right through the period. Indeed, nearly all the storms in the archive for the NH prior to WW2 are in the NA. Each of the SH basins (Figure 3) contribute to the contrasts described for the SH as a whole.

Overall, the annual numbers are relatively steady after about 1966, consistent with the arrival of satellite reconnaissance (Knutson et al. 2009). For the 30 knot criterion, the global annual average over the subsequent period 1967-2007 is 88.0 events (Table 1).

Despite the artificial variations in some basins, for the periods and cases included in Table 1, the ratio of the NH number to the SH number is typically a little over two. It remains larger than the ratio inferred from the SGP, in the two results quoted, the other two in Table 2 of Watterson et al. (1995), and also those from the climate model simulations of Ryan et al. (1992) and Hunt and Watterson (2009). Even in the most recent decade in IBTrACS (Table 1) the hemispheric ratio shows no decline.

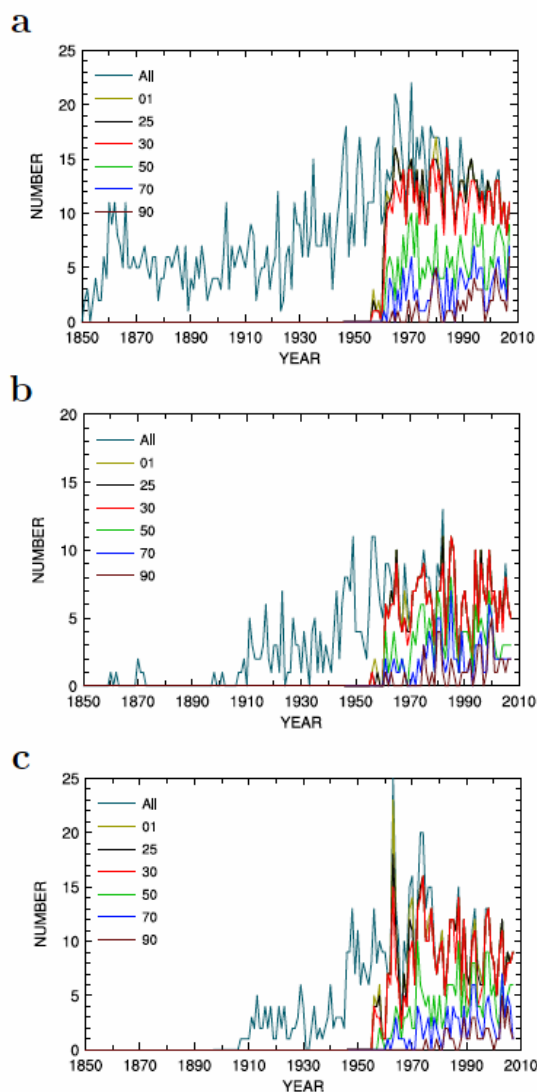


Figure 3. Numbers of cyclones for each year within SH regions (a) SIO, (b) NAR, and (c) WSP, for a range of speed criteria.

Numbers of Intense TCs

Further counts have been made of TC events that exceed larger MSW criteria. With the variation among measures of intensity used in different parts of the world, a simple uniform increment is used here, to give thresholds of 50, 70 and 90 knots. These speeds roughly correspond to Australian categories 2, 3, and 4 and U. S. hurricane categories 1, 2 and 3. Time series of annual numbers are included in Figs. 1, 2 and 3. Globally, for 1967-2007, these criteria produce 60%, 36% and 19%, respectively, of the number for 30 knots. The drops occur across all the basins. The ratio of NH to SH numbers over the

whole period increases a little with intensity (Table 1), but there is little indication of a difference in recent years (Table 2).

Table 2. Average number of intense TCs per year from IBTrACS, within each of three periods. The ratio of the NH to SH numbers is also given. The wind criterion is 90 knots.

Data	Globe	NH	SH	Ratio
1975-1989	14.9	11.2	3.7	3.00
1990-2004	19.9	13.7	6.3	2.18
2005-2007	23.0	15.7	7.3	2.14

With sea surface temperatures having risen over recent decades (e.g., Webster et al. 2005, or the website

www.metoffice.gov.uk/climatechange/science/monitoring), there is great interest in any corresponding changes in numbers or intensities of TCs (Knutson et al. 2009). Webster et al. (2005) presented time series of global, annual numbers over 1970-2004 for both tropical storms and U. S. category 1 events that appear similar to those for MSW 30 and 50 knots in Figure 1. They found rather little trend in these series, consistent with the small linear regression coefficient of 0.11 (events per year, per year) with standard error 0.12, in the IBTrACS series for MSW 30 knots over 1967-2007. Webster et al. (2005) then analysed the intense events in U. S. categories 4 and 5 and found increases between the averages for 1975-1989 and for 1990-2004, in each of six basins. The global number increased 57%. Kruk et al. (2008) did a similar analysis from IBTrACS and also found increases except for the WNP, and with a global increase of 30%.

A rigorous assessment of trends is beyond the scope of the present paper, but it is worthwhile to include some results based on the time series presented. Averages over the above 15-year periods for the 90 knot criterion are given in Table 2. Numbers increase in each hemisphere, and globally by 33%. They increase further in the latest three years (Table 2). Indeed, the global average in the last four years, 24.0 events per year, is rivalled only by 1991-4 (23.0 per year). The global trend over 1967-2007 is 0.28 (events per year, per year), which is statistically significant, given a standard error of 0.05. As a percentage, the increases are larger in the SH,

which suggests that data quality remains an issue, as argued by Landsea et al. (2006) and others (see Knutson et al. 2009). Certainly, variations in numbers in basins can be caused by regional variations in the conditions that promote genesis, as considered by Watterson et al. (1995), Pezza and Simmonds (2005), Chan (2007) and many other authors.

A Climatology of Cyclogenesis

Given the relatively stable numbers of events during the 41 years from 1967 to 2007, this period is used in a depiction of genesis locations. Numbers of storms that reached the MSW 30 knot criterion were accumulated on the global grid of 5-degree squares noted above. For comparison with earlier studies, the totals were scaled to a 20-year period (by multiplying by 20/41). The result for all seasons combined is shown in Figure 4.

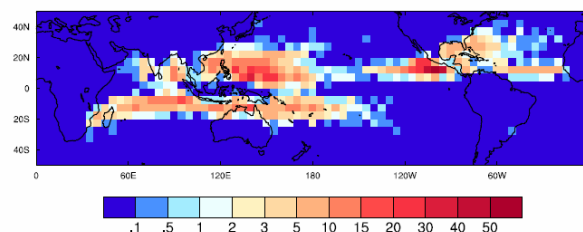


Figure 4. Numbers of genesis events per 20 years, within five degree squares, based on the 1967-2007 data for MSW criterion 30 knots, Annual case.

The first three colours represent squares with 0, 1 or 2 events over the whole period. As in earlier data sets, most genesis locations occur within 25°S and 30°N, the latitudes used to bound the basins in the Appendix. However, it can be seen that quite a few storms in IBTrACS have a first detection point farther north than 30°N in the North Atlantic. Some storms are traced back to squares that include land. Some others are traced to the squares next to the equator. Further assessment of the actual tracks and tropical characteristics of some storms may be warranted.

In any case, the spatial distribution is broadly consistent with that of the earlier data sets shown in Figure 2a and 2b of Watterson et al. (1995). Fewer events are counted in the Bay of Bengal, presumably related to the wind speed issue noted before for the NIO. Average numbers of events per single year for the various basins are given in

Table 3. Evidently, some five events per year in the NH have a genesis point outside the four northern basins, as defined here, and three events per year in the SH are outside the other three basins.

Table 3. Numbers of TCs per year (to the nearest integer) within each region (see Appendix), based on the 1967–2007 data for MSW criterion 30 knots. The Annual case represents the sum of the four seasons that follow.

Region	Annual	JFM	AMJ	JAS	OND
Globe	88	19	12	35	21
NH	59	1	8	35	15
SH	29	18	3	1	7
NIO	4	0	1	0	2
WNP	26	1	3	15	7
ENP	15	0	2	11	2
NA	9	0	1	6	2
SIO	11	7	1	0	3
NAR	6	4	1	0	1
WSP	9	6	1	0	2

The distribution of genesis in the four individual seasons is shown in Figure 5. The regional totals are also given in Table 3. For each hemisphere, some 60% of events occur in the (oceanic) summer season. The dominance of summer is particularly clear in the tropical Atlantic. Only for the NIO is summer not the most common season. Nearly all the remaining events occur in the seasons adjacent to summer.

Conclusions

The new IBTrACS archive is clearly a major achievement and it promises to enhance research into the global distribution of tropical cyclones. A single netcdf data file contains all recorded events, which are represented in a coherent format. Furthermore, it is the intention of the U.S. National Climatic Data Center to provide ongoing support for the archive, with semi-annual updates. The IBTrACS website states, nevertheless, that the data do not replace the official WMO best tracks for individual basins.

This paper considers only the distributions of cyclogenesis events, motivated by earlier work on the SGP. Time series of annual numbers are presented for the globe, both hemispheres and seven basin regions, through 2007. These are further partitioned by the maximum sustained wind achieved by each storm. Only in the North Atlantic ocean are all storms supplied with winds

reaching 30 knots, with a continuous, although likely incomplete, record back to 1851. The archive records storms over this period in the southern hemisphere, although wind speeds are not available until after 1956. In later decades the number of events in the NH is typically double that in SH, and this holds for more intense TCs also. The smaller ratio reported for the SGP appears to indicate an overestimation by that surrogate quantity in the south.

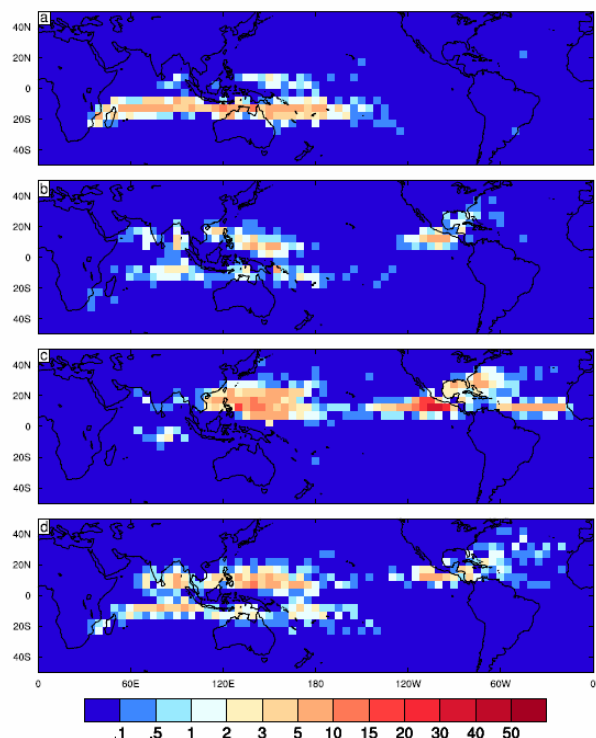


Figure 5. Seasonal numbers of genesis events per 20 years, as Fig. 4, for: (a) JFM, (b) AMJ, (c) JAS, and (d) OND.

Increases in the numbers of intense TCs in recent decades in IBTrACS are a little smaller than those reported elsewhere, but they continue. The global total in the years 2004–7 is not exceeded by any previous four-year period. Over the period 1967–2007, the trend in events reaching the 90 knot criterion represents a net increase of some 68%. The spatial distribution of genesis events averaged over that period is also presented. Both seasonal and annual distributions broadly concur with those in earlier studies.

While this work demonstrates the potential of the new archive, it also highlights the limitations to

what is known of cyclone occurrence, particularly prior to the satellite era.

Acknowledgements

This work contributes to the Australian Climate Change Science Program. Communication and encouragement from Ken Knapp of NCDC is acknowledged.

References

- Chan, J. C. L., 2007: Interannual variations of intense typhoon activity. *Tellus-A*, 59, 455–460. DOI:10.1111/j.1600-0870.2007.00241.x.
- Emanuel, K., 2005: Increasing destructiveness of tropical cyclones over the past 30 years. *Nature*, 436, 686–688. DOI:10.1038/nature03906.
- Gray, W. M., 1975: Tropical cyclone genesis. Dept. Atmos. Sci. report 234, 121 pp., Colorado State Univ., Fort Collins, CO.
- Hunt, B. G., and I. G. Watterson, 2009: The temporal and spatial characteristics of surrogate tropical cyclones from a multi-millennial simulation. *Clim. Dyn.* in press.
- Knapp, K. R., M. C. Kruk, D. H. Levinson, and E. J. Gibney, 2009: Archive compiles new resource for global tropical cyclone research. *Eos, Transactions, AGU*, 90(6), 46. 10.1029/2009EO060002.
- Knutson, T., C. Landsea, and K. Emanuel, 2009: Tropical cyclones and climate change: a review. *Global Perspectives on Tropical Cyclones: From Science to Mitigation*, World Scientific Publishing Co., Singapore. in press.
- Kruk, M. C., K. Knapp, D. Levinson, and J. Kossin, 2008: National Climatic Data Center global tropical cyclone stewardship. Abstracts of the 28th Conference on Hurricanes and Tropical Meteorology, Am. Meteorol. Soc., Boston, MA, 1–15.
- Landsea, C. W., 2007: Counting Atlantic tropical cyclones back to 1900. *Eos, Transactions, AGU*, 88(18), 197–200.
- Landsea, C. W., B. A. Harper, K. Hoarau, and J. A. Knaff, 2006: Can we detect trends in extreme tropical cyclones? *Science*, 313, 452–454. DOI:10.1126/science.1128448.
- Pezza, A. B., and I. Simmonds, 2005: The first South Atlantic hurricane: unprecedented blocking, low shear, and climate change. *Geophys. Res. Lett.*, 32, L15712. DOI:10.1029/2005GL023390.
- Ryan, B. F., I. G. Watterson, and J. L. Evans, 1992: Tropical cyclone frequencies inferred from Gray's

Yearly Genesis Parameter: validation of GCM tropical climates. *Geophys. Res. Lett.*, 19(18), 1831–1834.

Watterson, I. G., J. L. Evans, and B. F. Ryan, 1995: Seasonal and interannual variability of tropical cyclogenesis: diagnostics from large-scale fields. *J. Climate*, 8, 3052–3066.

Webster, P. J., G. J. Holland, J. A. Curry, and H.-R. Chang, 2005: Changes in tropical cyclone number, duration, and intensity in a warming environment. *Science*, 309, 1844–1846. DOI:10.1126/science.111644

APPENDIX

Ocean Basins

The basins used in the study are rectangular regions based on Gray's (1975) oceanic regions. The names and bounds listed here follow those of Watterson et al. (1995), except that because of the position of the grid squares, the effective longitudes are shifted 2.5° to the west.

<i>Label</i>	<i>Name</i>	<i>Latitudes</i>	<i>Longitudes</i>
NH	Northern Hemisphere	0°N, 90°N	2.5°E, 2.5°E
SH	Southern Hemisphere	90°S, 0°S	2.5°E, 2.5°E
NIO	North Indian	5°N, 30°N	62.5°E, 102.5°E
WNP	West North Pacific	5°N, 30°N	102.5°E, 177.5°E
ENP	East North Pacific	5°N, 30°N	142.5°W, 92.5°W
NA	North Atlantic	5°N, 30°N	92.5°W, 22.5°W
SIO	South Indian	25°S, 5°S	27.5°E, 102.5°E
NAR	Northwest Australian	25°S, 5°S	102.5°E, 142.5°E
WSP	West South Pacific	25°S, 5°S	142.5°E, 162.5°W